INORGANIC CHEMISTRY
FRONTIERS

REVIEW

View Article Online
View Journal | View Issue

Cite this: *Inorg. Chem. Front.*, 2024, **11**, 2212

Porphyrin-based MOFs for photocatalysis in water: advancements in solar fuels generation and pollutants degradation

Fangbing Liu,[a] Irene Rincón,[b] Herme G. Baldoví,[c] Amarajothi Dhakshinamoorthy,[c,d] Patricia Horcajada,[b] Sara Rojas,*[e] Sergio Navalón*[c] and Alexandra Fateeva*[a]

This review aims to provide a thorough summary of the versatile applications of porphyrin-based metal–organic frameworks (PMOFs) as photocatalysts in an aqueous environment, specifically focusing on the production of solar fuels and the degradation of pollutants. The first section describes the fundamental attributes of porphyrin molecules as building units of stable PMOFs, efficient in photocatalysis under solar light irradiation in water. Key considerations, such as their light absorption and photophysical properties, are discussed, and the structures of several representative PMOFs are detailed. The subsequent section highlights the utilization of PMOFs and composites for the photocatalytic hydrogen evolution reaction in the presence of sacrificial electron donors as well as for the overall water splitting into H_2 and O_2. The third section focuses on the versatile utilizations of PMOFs and composites in the photodegradation of different kinds of emerging organic pollutant, showing their potential for environmental remediation. Finally, this review summarizes the current state-of-the art of the field together with proposing insights into the future prospects and opportunities to reach more efficient materials to advance into the development of practical applications.

Received 29th September 2023,
Accepted 13th February 2024

DOI: 10.1039/d3qi01996a

rsc.li/frontiers-inorganic

A. Introduction

Porphyrins are tetrapyrrolic macrocycles where four pyrrole rings are linked by methyne bridges and, along with related compounds (corrins, chlorins), they represent an important class of molecules that are involved in life-essential processes such as breathing, photosynthesis and detoxification.[1,2] The most common examples in biology are undoubtfully heme and chlorophylls. The former is a ferrous protoporphyrin responsible for oxygen transport in haemoglobin, while the latter represents a class of pigments found in plants (usually magnesium complexes) enabling photosynthesis. There are also less common examples of naturally occurring porphyrins whose roles are still being investigated, such as bird feather pigments.[3,4] The key functions fulfilled by the porphyrinic molecules are enabled due to their unique structure and intrinsic properties. The aromaticity (18 conjugated π electrons) leads to strong visible light absorption and enhanced stability. Moreover, the ability to chelate various metal ions allows metalloporphyrin to bind and transport small molecules as well as perform redox processes.

Historically, complex unsymmetrical porphyrins that are naturally available were first discovered, structurally characterized and their synthesis attempted. Later, simpler octaethyl (bearing substituents on the β-pyrrolic positions) and tetraphenyl (bearing substituents at the methyne bridge meso positions) porphyrins were developed, leading to significant advancements in their chemical synthesis. As a result, on-demand functionalized molecules became accessible in terms of their increased-scale production and commercialization (examples of vendors: TCI chemicals®, Sigma-Aldrich®, Porphychem®). This progress greatly contributed to the development of porphyrin-based materials and devices, including metal–organic frameworks (MOFs). MOFs are appealing materials as they combine the intrinsic properties of porphyrins with their nanoscale structuring into a porous network, leading to high surface areas and accessibility of porphyrinic

[a]*Laboratoire des Multimatériaux et Interfaces, Université Lyon, Université Claude Bernard Lyon 1, UMR CNRS 5615, F-69622 Villeurbanne, France. E-mail: alexandra.fateeva@univ-lyon1.fr*
[b]*Advanced Porous Materials Unit, IMDEA Energy Institute, Avda. Ramón de la Sagra 3, 28935 Móstoles, Madrid, Spain*
[c]*Departamento de Química, Universitat Politècnica de València, C/Camino de Vera, s/n, 46022 Valencia, Spain. E-mail: sernaol@doctor.upv.es*
[d]*School of Chemistry, Madurai Kamaraj University, Madurai 625021, Tamil Nadu, India*
[e]*Department of Inorganic Chemistry, University of Granada, Avda. Fuentenueva s/n, 18071 Granada, Spain. E-mail: srojas@ugr.es*

sites. Although the first reports of porphyrin-based MOFs (PMOFs) date back to the 1990s,[5,6] stable and permanently porous solids were developed much more recently. Due to the commercial availability of the molecule, the majority of MOFs are currently based on the tetrakis(4-carboxyphenyl)porphyrin (TCPP) linker; however, PMOFs based on alternative functional groups are being increasingly explored to achieve novel architectures and physicochemical properties.[7]

Several recent reviews provide valuable perspectives in the field of PMOFs and highlight their significance.[8–10] The present review is focused on the remarkable advancements achieved in the relatively recent research topics involving the use of these MOFs for photocatalytic applications in aqueous media. Given the increasingly growing environmental pollution of air and water, sustainable photoactive materials are needed for developing renewable energy technologies. The fields of interest of this review concern water splitting for solar fuel generation and the photodegradation of organic pollutants in contaminated water. Consequently, fundamental aspects of hydrolytic stability are initially discussed, highlighting some examples of water-stable materials, and then light absorption and photophysical properties are introduced to rationalize the photocatalytic activity. The importance of structuring and elaborating composite materials to enhance the photocatalytic efficiency is addressed. Then, the application of PMOFs in the fields of water splitting and decontamination is discussed based on the most relevant examples to point out the achieved progress and the encountered limitations to finally suggest potential directions for further research.

Porphyrin-based MOFs and their water stability

The stability of PMOFs in aqueous environments is an absolute prerequisite to consider their application in water, which naturally aligns with the fundamental principles governing the hydrolytic stability of coordination networks. However, it is important to notice that some reports overlook this crucial concern and, in general, the stability tests are performed in very different conditions from one study to another (for example, amount of solid MOF per mL of aqueous phase, see below), hindering a direct comparison. Few recent reviews[11,12] give a very complete and insightful view on this topic, and only the main trends are briefly summarized below. Generally, MOFs' reactivity with water takes place on the coordination bond between the ligand and the metal. Its hydrolysis typically leads to the formation of a metal hydroxide and a protonated linker. Therefore, the metal–ligand bond strength is of paramount importance when considering aqueous stability. An estimation of this bond strength can be done based on the hard and soft acids and bases (HSAB) theory, wherein small ionic radius, high valent and low polarizable metal ions classically lead to stable frameworks when combined with hard ligands such as carboxylates. For this reason, MOFs based on trivalent and tetravalent metals (hard Lewis acids) are of high relevance in this review. Among those, some materials appear of special interest and their related structures are briefly described here. Three MOFs based on the TCPP linker stand out in the literature due to the relevance of their applications. The first water-stable MOF (in acidic and neutral pH aqueous solutions, tested with 10 mg of MOF in 10 mL deionized water) reported for the photocatalysis of the hydrogen evolution reaction (HER) was the Al-PMOF.[13] Its structure is formed by chains of hydroxo-bridged Al^{3+} octahedra that connect porphyrins in a stacked fashion (Fig. 1c). Later, a series of stable PMOFs based on Zr_6 clusters were reported; these MOFs present a very close composition but a topological diversity due to the variable connectivity of the Zr_6 nodes to the ligands. Among these, PCN-222 and PCN-224 structures are illustrated in Fig. 1a and b, respectively. As represented, PCN-222 displays a higher connectivity to the ligands compared with PCN-224 (8 *vs.* 6 ligands per node, respectively). PCN-222 is stable in aqueous acidic and neutral solutions (100 mg of MOF in 15 mL)[14] whereas PCN-224 is reported to be stable from pH 0 to 11 (500 mg of MOF in 10 mL).[15] Other related stable MOFs are reported such as MOF-525[16] (stable in acidic and neutral aqueous solution, 100 mg of MOF in 10 mL); however it can be noted that the latter one has been proposed as a disordered version of PCN-224.[17] More recently, an exceptionally stable MOF named MIL-173(Zr), based on Zr^{4+} and a different linker molecule, a polyphenolic porphyrin, was reported by some of us.[18] The inorganic secondary building unit (SBU) of MIL-173(Zr) is composed of a chain of edge-sharing ZrO_8 dodecahedra leading to a structure where the Zr coordination sphere is filled solely by the linker's oxygen atoms, unlike the previous cases where inorganic oxo or hydroxo co-ligands are present (Fig. 1d). Trihydroxyphenyl-porphyrins are arranged in a stacked manner and the framework is stable under acidic, neutral and basic pH (20 mg of MOF in 20 mL) as well as in coordinating phosphate buffer solution (0.01 M) for a week at 37 °C. From this last example, it appears important to note that, aside from the metal–ligand bond strength, factors such as the connectivity, geometry of the inorganic SBU and pore size also affect MOF stability. Indeed, extended SBUs often lead to more stable structures compared with the isolated metal sites or clusters, when larger pores structures can offer an easier water access for hydrolysis. Additionally, water stability is usually reported in solutions prepared using ultrapure water, while tests in the presence of coordinating anions found in real waters (*e.g.* sulfate, nitrate, chloride and carbonate anions) or even directly in wastewater, containing a variety of organic and inorganic species, are extremely scarce. Finally, the pH is important when considering hydrolytic stability; in the context of the applications of interest in this review, the stability of materials within the pH range 5 to 9 is particularly relevant.

Light absorption properties of porphyrins

In the field of MOFs as photocatalysts, porphyrinic chromophores are attractive ligands due to their strong absorption of light in the visible region. In Al- and Zr-based MOFs the metal orbitals are too high in energy to allow an efficient ligand to metal charge transfer.[19] For this reason, the optical properties and the frontier orbitals are primarily governed by the ligands

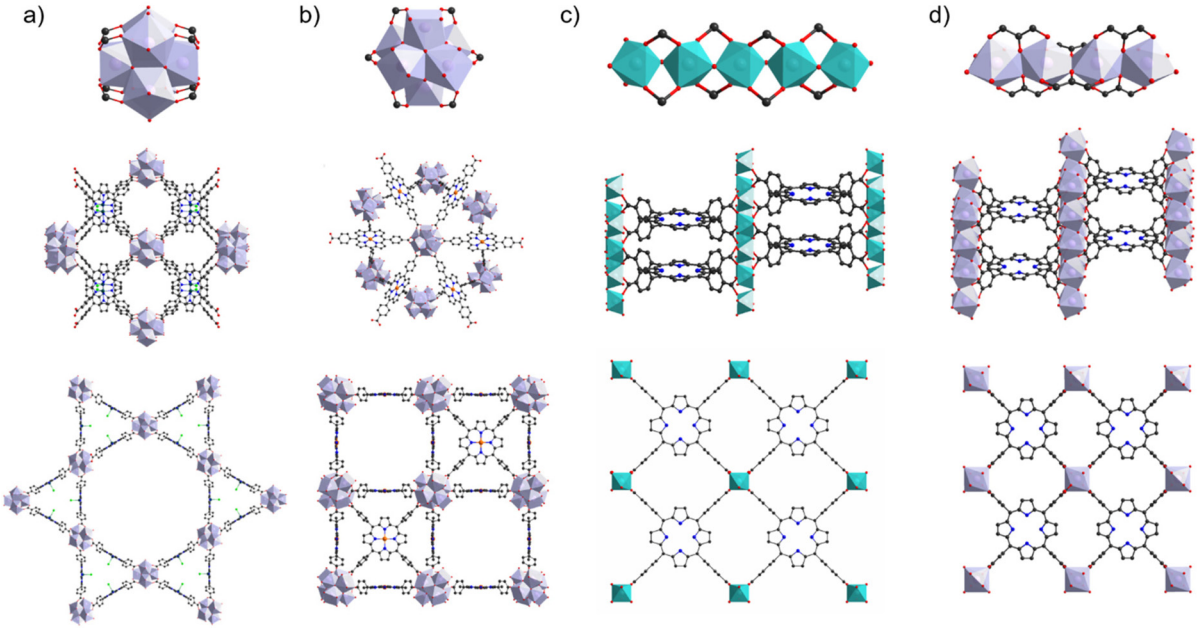

Fig. 1 Inorganic SBU and networks structures of PCN-222 (a), PCN-224 (b), Al-PMOF (c), and MIL-173 (d).

and their structuration inside the hybrid network.[20,21] Light-absorption properties of porphyrins are described by Gouterman's four-orbital model and correspond to the π–π* transitions.[22] They are affected by the nature of the organic substituents and the insertion of a metal inside the porphyrin core. Generally, the optical spectra of porphyrins display a very strong absorption band near to 400 nm, called the Soret band (molar extinction coefficients over 10^5 M^{-1} cm^{-1}), and several weaker Q bands in the region ranging from 500 to 700 nm (molar extinction coefficients over 10^4 M^{-1} cm^{-1}). Free-base porphyrins usually display four Q bands, while only two are commonly observed for metalloporphyrins due to the increase in symmetry upon metal coordination by the pyrrolic sites (Fig. 2a). Consequently UV-Vis spectroscopy is a suitable technique to assess the metal coordination inside the porphyrin.

Photocatalysis generalities using MOFs and PMOFs

In general, for semiconducting materials, photocatalytic activity arises from light absorption, with photons of an energy equal or greater to the band gap. Photoexcited electrons are transferred to the valence band while holes are in the conduction band. Then, the light-triggered charge separation pro-

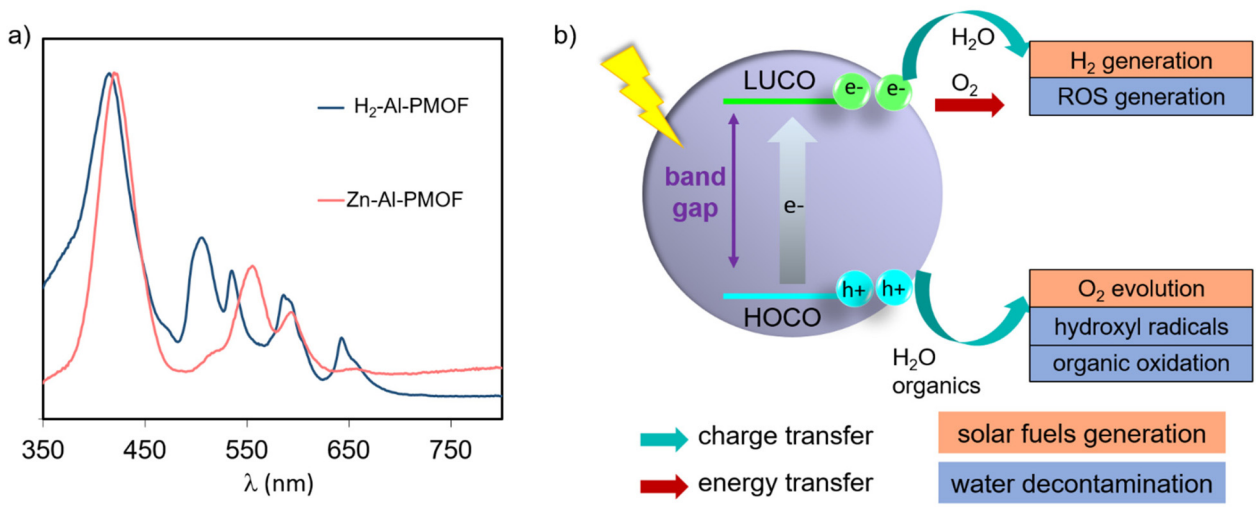

Fig. 2 Representative UV-Vis absorption spectra of the free-base and metalloporphyrin-based PMOF (a), and scheme of a photoinduced charge separation process and possible redox reactions at the interface of the photocatalyst (b).

cesses are followed by the migration of electrons and holes to the interface containing the substrate where the redox reaction can take place. Consequently, the activity of a material is dependent on the light-absorption properties and its energy band level diagram, as well as the electron and hole migration mechanism and kinetics. Regarding the energy band levels of MOFs, some authors have proposed to refer them as highest occupied crystal orbital (HOCO) and lowest unoccupied crystal orbital (LUCO), related to the valence and conduction band nomenclature used for inorganic semiconductors.[23,24] When charge separation occurs, generating electrons at the LUCO and holes at the HOCO, the charges can either react *via* redox reactions (Fig. 2b) or recombine in a radiative/non-radiative transition pathway. For solar fuel generation from water, the two processes of interest are proton reduction to H_2 (E° = 0 V *vs.* normal hydrogen electrode – NHE) and H_2O oxidation to O_2 (E° = 1.23 V *vs.* NHE). For example, photocatalytic overall water splitting (OWS) at pH 7 at 20 °C would require a HOCO maximum and a LUCO minimum of at least +0.82 and −0.41 V, respectively. Besides, it should be noted that, in some cases, an overpotential can be required in the HOCO and/or LUCO values to facilitate the OWS.[25] Regarding water remediation, several pathways can take place to proceed to the oxidative degradation of organic contaminants. The photogenerated holes located at the HOCO can act as oxidizers of organic substrates and they can also generate reactive hydroxyl radicals ($HO^\bullet$) by reacting with water. Additionally, the electrons located at the LUCO can induce the generation of reactive oxygen species (ROS) by either charge and/or energy transfer to oxygen molecules, producing highly reactive singlet oxygen and superoxide radical ($O_2^{\bullet-}$). On top of that, in the case of Fe-based MOFs, the Fenton effect can be utilized.[26] In this case, Fe^{2+} centres are also involved in generating the ROS when in presence of H_2O_2. Therefore, several pathways can be involved in the photocatalytic degradation of the large variety of contaminants, making the rationalization of the mechanism extremely complex. To reach photocatalytic activity, the frontier orbital positions must be compatible with the redox potentials of the aimed reactions to thermodynamically allow the process. Experimental evaluation of the band gap in MOFs is not a straightforward operation. For this reason, a computational approach is developed, being valuable not only to rationalize the photocatalytic properties but also to design materials with engineered properties. In this perspective, density functional theory (DFT) calculations have been implemented to assess the impact of the PMOF composition in terms of the metal inside the porphyrin core[27] or in the inorganic SBU of the framework[28,29] and various alterations of the porphyrin ligand[29] on the band gap of the material. A computational approach is also used to help in understanding the electron–hole relaxation pathways.[30]

Indeed, from the experimental results, the main challenge towards efficient photocatalysis is the radiative charge recombination of the electrons and holes, generating a light emission instead of the sought-after redox activity. To overcome this issue, numerous studies use sacrificial electron donors (SED) that are reducing agents (*e.g.* methanol, triethanolamine (TEOA)). Their role is to fill the vacancy in the HOCO that will prevent the charge recombination, but then only the reductive pathway from the electrons at the LUCO can take place. In this context, the majority of studies have reported the use of SED as an appropriate strategy to boost the HER.[24] Regarding water splitting, the oxygen evolution reaction (OER) represents the most thermodynamic and kinetically demanding half-reaction of the process.[31] Similarly, sacrificial electron acceptors (*e.g.* Ag^+, $S_2O_8^{2-}$) can be used to evaluate the photocatalytic performance of the OER. It is thus evident that using both holes and electrons without sacrificial agents is a true challenge to exploit the full activity of the photocatalyst and accomplish both reduction and oxidation reactions for OWS.

PMOF-based composite systems for photocatalysis

An alternative strategy for limiting the electron–hole recombination is to spatially separate them by elaborating a heterojunction composed of two photocatalytic materials. Given that the electron or hole migration through the heterojunction is favourable, the two types of charge carrier would be located at different materials, thus making their recombination much harder. In the field of solar fuel generation, a common strategy consists of the modification of the photocatalyst with metal nanoparticles (NPs). NPs such as Pt or Co_3O_4 act as efficient and selective co-catalysts for proton reduction and water oxidation, respectively. However, the implementation of precious metals presents drawbacks regarding their cost and availability, and some co-catalysts such as Pt NPs can also catalyse the back-reaction of H_2 and O_2 recombination to water, decreasing the efficiency of the process.[24]

Recently, 2D PMOFs have attracted increasing attention for their applications in catalysis. Importantly, 2D MOFs are particularly well-suited for the elaboration of MOF-based composites, by combining these MOFs with other advanced 2D materials such as graphene, polymers and transition metal dichalcogenides. The 2D topology can facilitate diffusion and the accessibility of active sites as compared with 3D microporous structures.[32,33] Moreover, 2D MOFs can present increased semiconducting behaviour that is beneficial for the charge carriers' mobility in catalysis.[34,35] This topology is obtained either from a top-down or bottom-up approach.[36,37] In the former, an exfoliation (mechanical or chemical) of a 3D network is performed when in the latter one, 2D MOFs are directly obtained during the synthesis. Directing the synthesis to 2D morphology may be achieved by using substrates, surfactants or interfacial synthesis. As discussed below, this strategy is particularly explored in the most recent studies regarding water decontamination.

B. Solar fuel generation

Solar fuels refer to small molecules obtained through the redox reactions of H_2O, CO_2 or N_2 such as H_2, C_1 or C_{2+} products and NH_3, respectively.[38,39] This review is limited to

solar fuel generation through photocatalytic water splitting using PMOFs; however, it is important to highlight that PMOFs have also been used as photocatalysts for CO_2 reduction in the presence of water, as recently reported in numerous studies and reviews,[40–46] and activity for N_2 reduction was also reported.[47]

The following sections will now focus on the photocatalytic performance of PMOFs for water splitting into H_2 and/or O_2.

MOFs as photocatalysts for water splitting

Generally, an efficient reaction mechanism in MOF-based photocatalysts is governed by a ligand-to-metal charge transfer (LMCT) process. Here, the irradiation of a MOF photocatalyst with photons of energy equal to or higher than its band gap results in the photoejection of electrons from the organic ligand to the metal ions present in the SBU. The reader is referred to some reviews dealing with other possible mechanisms in MOFs including metal-to-metal charge transfer, ligand-to-ligand charge transfer or metal-to-ligand charge transfer, among other possibilities.[24,48,49]

In contrast to inorganic semiconductors, most of the reported MOFs, including PMOFs as photocatalysts for water splitting, are poor electron conductors or even classified as insulator materials.[49] Photoexcitation of a common semiconductor results in an increase of electrical conductivity compared with its insulating character in the ground state. In the case of most MOFs, the mobility of charge carriers is more limited. Regardless of their relatively low electrical conductivity, MOFs can undergo electron/hole pair separation upon irradiation and promote redox reactions such as the OWS. Some authors have proposed to consider MOFs as an arrangement of metal complexes that undergo charge separation without significant charge migration upon photoexcitation, enabling the redox reactions.[23]

An important aspect when performing a photocatalytic reaction is to evaluate its efficiency in terms of the conversion of light energy into chemical energy. One of the most commonly used parameters to estimate the performance of solar-driven photocatalytic HER or OWS systems is the so-called solar-to-hydrogen (STH) conversion efficiency η_{STH}.[24,25,50] As detailed in the three equations below, STH refers to the amount of incident solar energy that is converted into H_2. Some studies have proposed that those photocatalytic systems with an STH of about 10% and a minimum lifetime of operation of ten years would have potential industrial application.[50] Among the most active and stable photocatalysts, the aluminium-doped strontium titanate (Al:$SrTiO_3$) solid modified with co-catalysts ($RhCrO_x$, MoO_y) was recently tested in photocatalytic solar panels at a 100-m^2 scale, reaching an STH of 0.76%.[51] Regarding MOF-based photocatalysts for the OWS, up to now the highest achieved STH efficiencies remain below 0.1%.[24] However, to put things in perspective, it is important to note that the field of inorganic photocatalysts for water splitting is under continuous development since 1972[52] while the first use of MOFs for OWS was reported in 2017.[23] Considering the dynamic progress in the field of MOFs, much higher efficiencies are expected to be achieved in the short- and mid-term.

$$\eta_{STH}(\%) = \left[\frac{\text{produced chemical energy}}{\text{solar energy input}}\right] \times 100$$

$$\eta_{STH}(\%) = \left[\frac{\text{rate of } H_2 \text{ production} \times \Delta G_{H_2O \rightarrow H_2 + \frac{1}{2}O_2}}{\text{total incident solar power} \times \text{electrode area}}\right]$$

$$\eta_{STH}(\%) = \left[\frac{(\text{mmol of } H_2 \text{ per s}) \times (237000\ \text{J mol}^{-1})}{P_{total}(\text{mW cm}^{-2}) \times \text{area (cm}^2)}\right]_{AM1.5G}$$

Another parameter employed to study the photocatalytic performance of a material during the HER or OWS is the apparent quantum yield (AQY) efficiency.[24,50] This parameter aims to estimate the photocatalytic activity of a material in terms of the number of reacted electrons over the number of the incident photons emitted at specific monochromatic wavelengths, according to the following equations:

$$\text{AQY}(\%) = \frac{\text{number of reacted electrons}}{\text{number of incident photons}} \times 100$$

$$\text{AQY}(\%) = \frac{2 \cdot \text{number of hydrogen molecules evolved}}{\text{number of incident photons}} \times 100 = \frac{2 \cdot \eta_{H2,t} \cdot N_A \cdot h \cdot c}{P \cdot S \cdot \lambda_{inc} \cdot t} \times 100$$

where $\eta_{H2,t}$ is the number of H_2 moles evolved during the duration t (s) of the incident light exposure, N_A is Avogadro's constant, h (J s^{-1}) is the Planck constant, c (m s^{-1}) is the speed of light, P (W m^{-2}) is the power density of the incident monochromatic light, S (m^2) is the irradiation area and λ_{inc} is the wavelength of the incident monochromatic light.

The aforementioned, modified aluminium-doped strontium titanate presents an AQY of 56% at 365 nm, and due to the broad visible light absorption, a PMOF-based system has been reported to perform OWS with an AQY of 1.5% at 436 nm.[53]

Turnover number (TON) and turnover frequency (TOF) values are also sometimes provided in the reports. The TON refers to the number of moles of substrate reacting per number of moles of the active sites in a catalyst, while the TOF measures this ratio over a certain time. TOF is a commonly used parameter in (photo)catalysis; however, identifying and accurately quantifying the number of active sites in a photocatalyst is often an intricate and challenging task.

The field of MOFs as photocatalysts for water splitting is still in its infancy and the majority of investigations report the efficacy of the systems in terms of micromoles of H_2 or O_2 per gram of photocatalyst and, to a much lesser extent, the AQY or STH values are estimated.[24] It should also be considered that the majority of investigations involve the use of small quantities of photocatalyst, typically from 5 to 50 mg. It is important to recognize that the scale-up of the same photocatalytic setup to, for example, 1 g of photocatalyst, may result in a significant variation of the photocatalytic activity. Indeed, the use of higher or lower quantities of photocatalyst may generate light scattering or incomplete irradiated light absorption, respectively. A good practice in the field would be to evaluate

the influence of the photocatalyst amount using a particular photocatalytic system, and report the results in terms of micromoles or millimoles of products using these specific conditions instead of referring to the mass of used catalyst.[54] In some cases, the photocatalytic activity is reported as μmoles g^{-1} h^{-1}, which is determined based on the initial rate of H_2 production or the production observed after several hours. Special care must be taken when considering activities estimated using these methods, since in most cases the production of H_2 and/or O_2 is not linear over time. The non-linearity can be associated with the accumulation of H_2 and O_2 within the MOF pores, leading to a spontaneous back water-splitting reaction.[24]

The first use of MOFs as photocatalysts for the HER was reported in 2010 by García and co-workers: they used water-stable Zr^{4+} terephthalate-based MOFs with UiO-66 topology in the presence of methanol as a sacrificial electron donor and UV-Vis light irradiation.[55] The higher photoactivity of Zr-UiO-66(NH_2) *vs.* Zr-UiO-66 solid was associated with the functionalization of the aromatic ring from the terephthalate ligand with amino groups in the former one, resulting in a new absorption band from about 310 to 440 nm. The estimated AQY of Zr-UiO-66(NH_2) and Zr-UiO-66 were 3.5 and 0.1%, respectively, when irradiating with monochromatic light of 370 nm. For both solids, deposition of Pt NPs as co-catalyst further increased the photoactivity for the HER. Transient absorption spectroscopy (TAS) using a laser excitation at 355 nm confirmed the formation of long-lived (>300 microseconds) electron/hole pairs in both solids. Since this original publication, the number of examples reporting the use of MOF-based materials as photocatalysts for the HER has been continuously increasing. The reader is referred to some excellent reviews for more detailed information of the achievements made in this area.[24,42,56–62] Some of the widely reported photocatalysts for this purpose are terephthalate-based MOFs frequently modified with functional groups to enhance the visible light absorption. However, most of these photocatalysts have an onset of visible light absorption below 500 nm, a fact that hampers harvesting an important fraction of solar light irradiation to promote the photocatalytic HER.[24,50,63]

Photocatalytic HER using PMOFs

Aiming to overcome the aforementioned limitation, several studies have reported the use of PMOFs as photocatalysts for this purpose.[8,64] One of the salient properties of PMOFs is their ability to absorb visible light and thus increase their efficiency towards a solar-driven HER.[24,39,46,65] In a pioneering study, Rosseinsky and co-workers reported in 2012 the first example of the use of water-stable Al^{3+}-based PMOFs as a photocatalyst for the HER.[13] The MOF was prepared by hydrothermal synthesis using a free-base H_2TCPP and $AlCl_3{\cdot}6H_2O$. The resulting material consisted of a porous (Brunauer–Emmett–Teller surface area-S_{BET} = 1400 m^2 g^{-1}) red solid, H_2TCPP[AlOH]$_2$ (referred to as Al-PMOF or Al-TCPP, Fig. 1c). The UV-Vis diffuse reflectance spectrum of the MOF shows the presence of the Soret band at 415 nm accompanied by four Q bands at lower energy, as expected from the porphyrin ligand of the MOF (Fig. 2a). Importantly, the free-base H_2-Al-PMOF resulted in photocatalytic stability for the HER under visible light irradiation, in the presence of an SED and Pt colloidal solution as co-catalyst (Table 1, entry 1). This material was then modified by inserting Zn^{2+} inside the porphyrin core; however the resulting photoactivity appeared to be relatively lower. Since this report, the number of experimental and theoretical studies about the development of PMOFs for water splitting is unceasingly growing.

In a related study, Al-PMOF was metalated with Pt single atoms that resulted in 30 times higher photoactivity for the visible-light driven photocatalytic HER (TOF = 35 h^{-1}) compared with the Pt NPs supported on Al-PMOF[66] (Fig. 4).

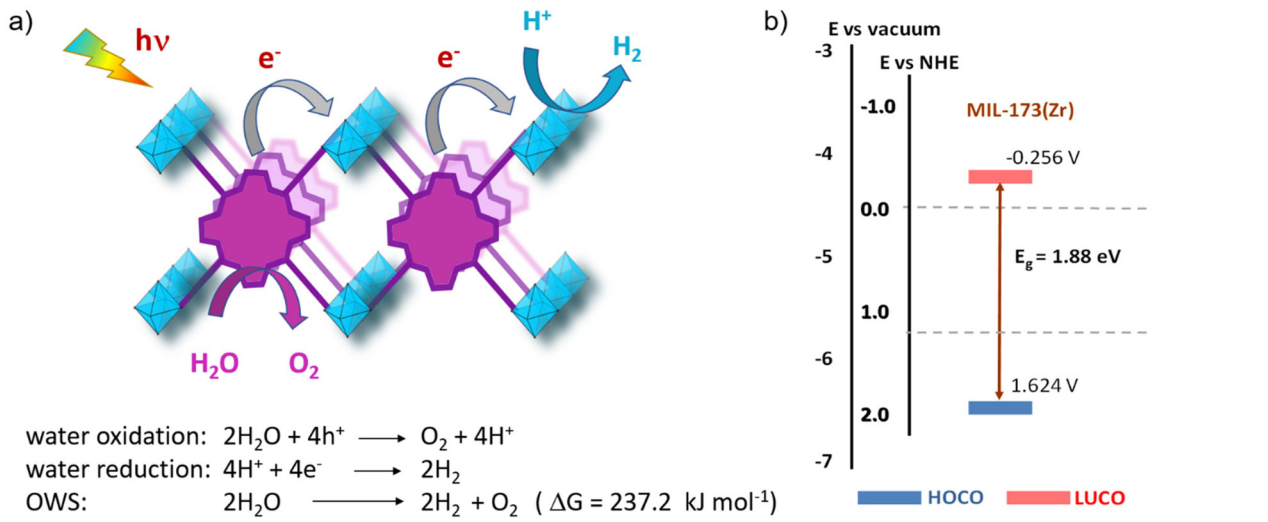

Fig. 3 General mechanism of photoinduced charge separation in MOFs triggered by light absorption and photoinduced charge transfer to the near metal node with the associated half and overall water splitting reactions equations (a), and energy level diagram for the PMOF MIL-173(Zr) (b).

Table 1 Summary of selected examples using PMOFs as photocatalysts for the HER

Photocatalyst	Reaction conditions	Activity	General remarks	Ref., year
Al-PMOF based on TCPP ligand	Photocatalyst (3.5 mg), ethylenediaminetetraacetic acid solution (35 mL; 0.0215 M), colloidal Pt (10 mM), pH 5.5 using sodium citrate, visible light source (300 W, λ > 420 nm filter), 8 h	1 mmol g^{-1}	The photocatalyst is stable after use based on XRD and SEM	13, 2012
Al-TCPP-Pt	Photocatalyst (5 mg), CH_3CN (18 mL), H_2O (1 mL), TEOA (1 mL), visible light irradiation (300 W Xe lamp equipped with a UV cut-off filter, λ > 380 nm), 4 h	0.129 mmol g^{-1} h^{-1}	The photocatalysts retains its activity and stability (XRD, TEM, STEM), for four consecutive uses	66, 2018
PtSA-MNSs based on TCPP-Cu MOF	Photocatalyst (5 mg), H_2O solution (0.1 M ascorbic acid), visible light irradiation (300 W Xe lamp equipped with a 420 nm cut-off), 5 °C, 5 h	11.32 mmol g^{-1} h^{-1}	The solid can be reused without significant loss of activity and maintains most of its initial structure	68, 2019
USTC-8(In)	Photocatalyst (10 mg), CH_3CN (23 mL), H_2O (1 mL), trimethylamine (2 mL), H_2PtCl_6 (Pt content: 1.5 wt%), irradiation source (300 W, λ > 380 nm filter)	0.3413 mmol g^{-1} h^{-1}	The photocatalyst is stable after 2 h based on XRD. The activity is maintained after 5 uses (2 h per cycle)	67, 2018
Zr-PCN-222(Pt)	Photocatalyst (10 mg), reaction solution (CH_3CN : TEOA : H_2O 18 : 2 : 0.4), visible light irradiation ($\lambda \geq 400$ nm), 4 h	0.351 mmol g^{-1} h^{-1}	The activity (~20%) and stability of the used photocatalyst decreased	69, 2021
Zr-PCN-222(Pt, 4.7%)	Photocatalyst (5 mg), H_2O (90 mL), TEOA (10 mL), visible light irradiation (300 W Xe lamp, λ > 420 nm), 6 °C, 5 h	0.614 mmol g^{-1} h^{-1}	The photocatalyst can be reused, retaining most of its activity and structural integrity	70, 2022
Zr-TCPP-bpydc	Photocatalyst (50 mg), H_2Cl_6Pt (1 wt%), TEOA (100 mL, 10%), visible light irradiation (300 W lamp with 420 nm cut-off filter), 4 h	213.68 μmol g^{-1} h^{-1}	The photoactivity is mostly maintained (96.04%) after four consecutive uses. The reused catalyst is stable based on XRD, FTIR and SEM analyses	73, 2022
CdS@PCN-222(Pt)	Photocatalyst (2 mg of supported CdS), H_2O (10 mL), lactic acid (1 mL), visible light irradiation (300 W Xe lamp, λ > 420 nm filter), 5 h	71.65 mmol g_{CdS}^{-1} h^{-1}	The activity and MOF stability slightly decrease upon reuse	71, 2023
Pt@Pd-PCN-222(Hf)	Photocatalyst (5 mg), CH_3CN (10 mL), TEOA (2.5 mL), H_2O (0.25 mL), visible light irradiation (300 W Xe lamp, λ > 420 nm filter), 3 h	22.674 mmol g^{-1} h^{-1}	The photocatalyst can be reused three times (6 h per cycle) without loss of activity. TON 4131.2	72, 2019
$[(\iota'\text{-}SCH_2)_2NC(O)C_5H_4N]^-[Fe_2(CO)_6]$ into Zr-PMOF	Photocatalyst (0.002 mM of iron subunit), ascorbic acid (20 mmol), pH 5 (1.0 M acetate buffer solution), visible light (300 W lamp, λ > 420 nm), 2 h	3.8 μmol after 2 h	The photocatalytic activity reached a plateau after 2 h	74, 2014
Pt-PMOF(Ti)	Photocatalyst (10 mg), H_2O (270 mL), ascorbic acid (10 mmol), visible light irradiation (300 W, λ > 420 nm), 5 h	8.52 mmol g^{-1} h^{-1}	The photocatalyst is stable upon reuse. AQY of 0.26% at 400 nm	79, 2019
Pt@Ti-PMOF based on TCPP ligand	Photocatalyst (5 mg), aqueous solution (50 mL; ascorbic acid, 1 M), 10 °C, visible light irradiation (300 W Xe lamp, λ > 420 nm filter), 5 h	15.5 mmol g^{-1} h^{-1}	It retains most of its initial photoactivity for 3 consecutive uses (5 h per cycle). The reused photocatalyst was not characterized	96, 2022
Ru-TBP-Zn	Photocatalyst (0.1 mg), CH_3CN (2.0 mL), H_2O (0.1 mL H_2O), TEOA (0.5 mL), visible light irradiation (230 W lamp, λ > 400 nm filter), 5 h	0.24 mmol h^{-1} g^{-1}	The photocatalyst maintains its activity and structure after six consecutive uses	80, 2018
HNTM-Ir/Pt; Zr-PMOF hollow nanotubes	Photocatalyst (50 mg), CH_3CN (45 mL), H_2O (1 mL), TEOA (4 mL), visible light source (300 W Xe lamp, λ > 400 nm filter), 5 °C, 5 h	0.202 mmol g^{-1} h^{-1}	The photocatalyst is stable for 3 consecutive uses based on PXRD, TEM and ICP	76, 2018

Incorporation of Pt allowed both trapping electrons and acting as a co-catalyst for the HER. Photocurrent (PC) (Fig. 4b) and electrochemical impedance spectroscopy (EIS; Fig. 4c) studies indicated that the metalation of Al-PMOF with Pt single atoms favours the photoinduced charge separation and reduced the charge transfer resistance. In addition, results from ultrafast TAS showed that the presence of Pt in the Al-PMOF favoured the spatial separation of the photoinduced charge carriers with the subsequent increase of photocatalytic activity. DFT calculations further revealed that the presence of a Pt single atom in Al-PMOF is favourable in terms of the hydrogen atom binding energy and contributes to enhancing the H_2 production. This study exemplifies the possibility to boost the photocatalytic activity of Al-PMOFs by single-atom metalation compared with the traditional strategy of depositing metal NPs on or within the photocatalyst structure.

Alternatively, a study reported an isotopic compound of Al-PMOF based on In inorganic units, [USTC-8(In)].[67] Contrary to the case of Al, In can be coordinated by the pyrrolic porphyrin sites, lying out-of-plane of the porphyrin ring (Fig. 5b). The MOF exhibits high photocatalytic activity and stability for the HER. Besides, insertion of divalent metals inside the porphyrin core was performed (USTC-8(M), M = Cu^{2+}, Co^{2+}, Ni^{2+}); these cations lie in the plane of the porphyrin ligand. Fig. 5a

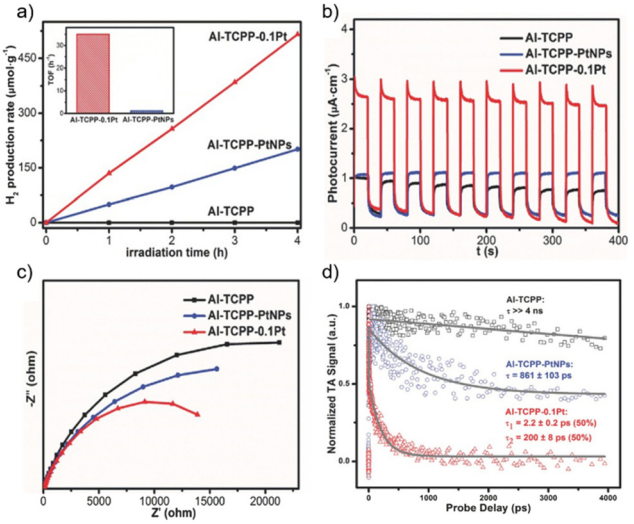

Fig. 4 (a) Photocatalytic H_2 production rates of Al-TCPP, Al-TCPP-PtNPs, and Al-TCPP-0.1Pt (inset: the calculated TOFs of Al-TCPP-PtNPs and Al-TCPP-0.1Pt). (b) Photocurrent responses, (c) EIS Nyquist plots and (d) comparison of the ultrafast TA kinetics (pump at 400 nm and probe at 540 nm) for Al-TCPP, Al-TCPP-PtNPs, and Al-TCPP-0.1Pt. Reproduced from ref. 66 with permission from *Wiley-VCH*, copyright 2018.

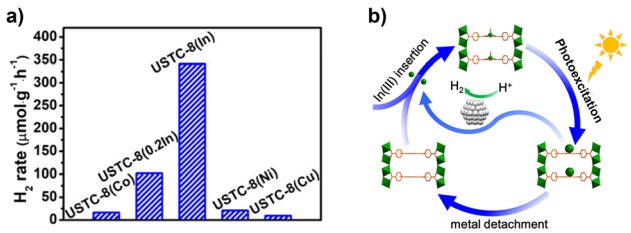

Fig. 5 (a) Photocatalytic H_2 production *via* water splitting over different MOFs. (b) Proposed detachment–insertion mechanism of USTC-8(In) during the photocatalytic recycling. Reproduced from ref. 67 with permission from *American Chemical Society*, copyright 2018.

shows that USTC-8(In) outperforms the counterparts based on divalent metalloporphyrins. PC and EIS measurements allowed the conclusion that USTC-8(In) presents the most efficient photoinduced charge separation and lower charge transfer resistance of the series. Regarding the reaction mechanism, photoinduced electron transfer from the ligand to the central metal atom of the porphyrin was proposed. The photogenerated holes were consumed by trimethylamine acting as an SED. The electron transfer would result in the reduction of In^{3+} ions leading to the increase of the ionic size and facilitating its detachment from the porphyrin core. This hinders e^-/h^+ recombination and favours electron transfer to colloidal Pt NPs in the reaction medium, promoting the HER. Experimental evidence about indium detachment was obtained by monitoring the changes of the UV-vis absorbance signal of USTC-8(In) suspension. The photocatalytic HER using USTC-8(In) solid was maintained upon five consecutive uses without changing the reaction vessel. In contrast, if the photocatalyst was recovered by centrifugation, its catalytic activity dropped by about 25% in the second cycle, which was attributed to In detachment from the porphyrin. Interestingly, immersing the solid in a solution of indium nitrate allowed it to almost recover its initial photocatalytic activity. This study exemplifies the possibility of tuning the photocatalytic activity of PMOFs by taking advantage of the intrinsic coordination properties of the porphyrin core with trivalent metal ions.

Together with the experimental progress, theoretical studies have considered the impact of PMOFs' composition on the electronic properties, for example by metalation of the porphyrin ligands.[27,28] Fig. 6 summarizes the influence of porphyrin metalation in Al-PMOFs on the resulting band gap and band edge position values.[27] These results show that Co^{2+}, Ni^{2+}, Cu^{2+} and Zn^{2+} metalated TCPP-based MOFs exhibit favourable band gap values for solar light absorption and band edge alignment for water splitting into H_2 and O_2. In contrast, metalation with Fe^{2+} ions results in a material with a valence band position above the thermodynamically required one for water oxidation.

PMOFs of different topology have been studied for the HER; in particular, Pt-TCPP ligand was coordinated to Cu dimers arranged in paddle-wheel clusters to achieve MOF nanosheets (MNSs) exhibiting Pt single atoms: PtSA-MNSs[68] (Fig. 7). Ultrathin 2D PMOF nanosheets (2.4 ± 0.9 nm; S_{BET} = 570 $m^2\ g^{-1}$) were elaborated *via* a surfactant-assisted synthesis. The solid, having a 12 wt% of Pt single atom, exhibited excellent photocatalytic activity (11 320 μmol $g^{-1}\ h^{-1}$) and good

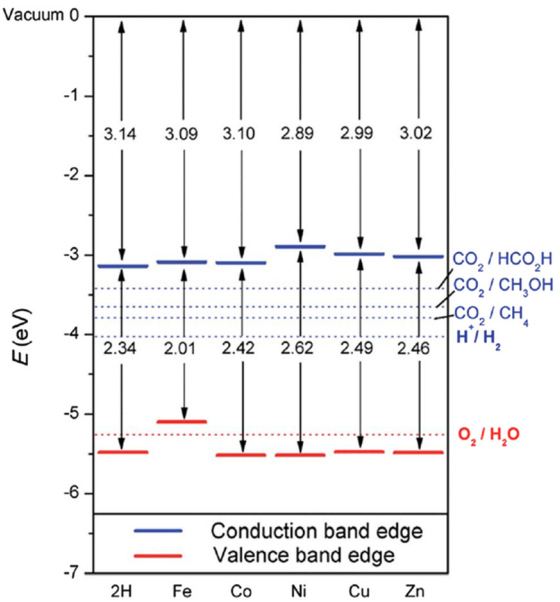

Fig. 6 Bandgaps and band edge positions with respect to the vacuum level, as calculated with the HSE06 functional. Energy levels corresponding to redox potentials of water splitting and carbon dioxide reduction reactions producing methane, methanol, and formic acid at pH 7 are also shown with dotted lines. Reproduced from ref. 27 with permission from the *Royal Soceity of Chemistry*, copyright 2015.

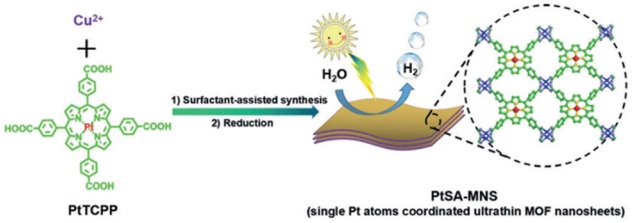

Fig. 7 Illustration of the synthetic route for the preparation of PtSA-MNSs through a surfactant-stabilized coordination strategy. Reproduced from ref. 68 with permission from *Wiley-VCH*, copyright 2019.

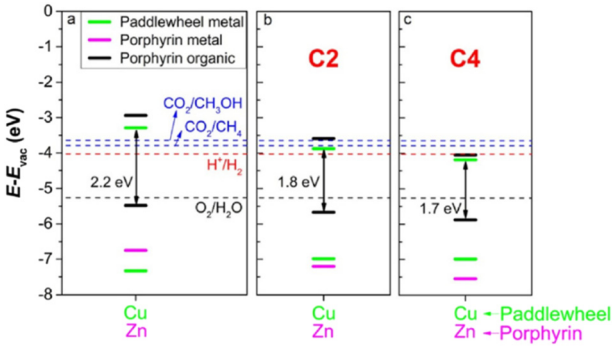

Fig. 8 (a) Comparison between band alignments of the Cu-ZnTCPP, (b) Cu–Zn–C2 and (c) –C4 systems. The bands of metal at the paddlewheel, metal at the centre and organic atoms of porphyrins (C, N and H) are shown in green, magenta and black, respectively. The energy levels of relevant half-reactions involved in water splitting and CO_2 reduction to CH_4 and CH_3OH are also shown. Reproduced from ref. 29 with permission from *IOP Publishing*, copyright 2021.

stability for the HER under visible light irradiation (Table 1). For comparison, the use of Pt NPs (11.8 wt%) supported on MNSs or MNSs alone resulted in much lower activities with the values of 317 and 2.0 μmol g^{-1} h^{-1}, respectively. The superior performance of PtSA-MNSs was ascribed to its efficient photoinduced charge separation, as revealed by PC and EIS measurements. DFT calculations further supported the benefits of single Pt atoms in the solid to favour hydrogen atom binding and electron transfer toward an efficient photocatalytic HER. The photocatalyst retains most of its initial activity (>93%) after 4 consecutive cycles (5 h per cycle). The reused solid was stable based on powder X-ray diffraction (XRD), transmission electron microscopy (TEM) and scanning transmission electron microscopy (STEM) while the Pt loading decreased upon reuse from 12 to 10.9 wt%.

In a related computational work, DFT and time-dependent DFT simulations were applied to a series of 2D PMOFs based on M-TCPP (M = Zn or Co) and paddlewheel clusters (Co, Ni, Cu or Zn) with the aim to optimize the photocatalytic activity for water splitting.[29] The study indicated that photocatalytic activity may be effectively achieved by adopting any of the three following strategies: (1) appropriate modification of band alignment by optimizing the metal centre either at the paddlewheel or at the porphyrin core position; (2) increasing the absorption of visible light by partial reduction of the porphyrin unit to chlorin; and (3) replacing the benzene group between the porphyrin and the paddlewheel by ethyne (C2 in Fig. 8) or butadiyne (C4 in Fig. 8) groups to alter the linker to metal charge transfer. Nevertheless, it should be observed that strategies derived from the computational methods may be challenging for experimental implementation.

As discussed in the introduction, Zr-based PMOFs represent an important class of materials for photocatalytic applications. In a series of reports, water-stable Zr/Hf-PMOFs, such as the PCN-222 framework, have been selected as photocatalysts for the HER (Table 1). The main modifications of these PMOFs to boost their activity include metalation of the porphyrin core[69–72] and/or modification with metal NPs[71–73] and, in a lesser extent, incorporation of metal complexes[74] within their structure. As previously discussed for the case of Al-PMOF, metalation of the porphyrin in PCN-222 with single Pt atoms resulted in a photocatalyst with higher activity for the HER compared with the use of Pt NPs, which is associated with the higher photoinduced charge carrier efficiency of the former (Fig. 9).[70] The estimated AQY of this photocatalyst at 420 nm was 1.05%. Besides, the photocatalyst could retain about 93% of its initial activity after 4 uses (5 h per cycle) and exhibit similar features to the pristine material based on PXRD, scanning electron microscopy (SEM), Fourier transform infrared spectroscopy (FTIR), and X-ray photoelectron spectroscopy (XPS) studies, while inductively coupled plasma optical emission spectroscopy (ICP-OES) showed a slight decrease in the Pt content (4.3 *vs.* 4.7 wt% for the fresh sample). The higher photocatalytic activity of PCN-222(Pt) *vs.* PCN-222 is due to the more efficient charge separation as revealed by several spectroscopic techniques like photoluminescence (PL) and EIS as well as PC measurements. Interestingly, electron paramagnetic resonance (EPR) spectroscopy showed the formation of a new signal attributed to the formation of Zr^{3+} when using PCN-222. The signal intensity increased in the case of PCN-222(Pt) due to the better photoinduced charge separation from the Pt-porphyrin ligand to the Zr^{4+} oxo clusters. Regardless of the presence of dual catalytic centres in the PCN-222(Pt) and based on the achieved photocatalytic results, it was proposed that the

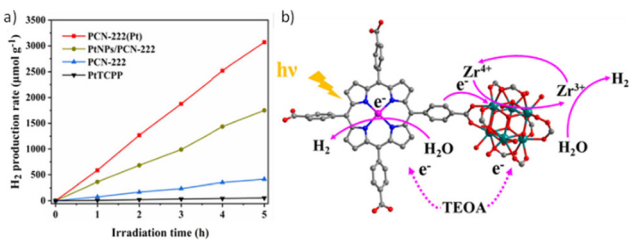

Fig. 9 (a) Photocatalytic H_2 production rates of PtTCPP, PCN-222, PtNPs/PCN-222, and PCN-222(Pt). (b) Proposed photocatalytic mechanism of dual catalytic centres in PCN-222(Pt). Reproduced from ref. 70 with permission from the *Elsevier*, copyright 2022.

presence of Pt single atoms in the porphyrin ligand is the main factor responsible for electron capture and the active site for the HER.

In a related study, Zr-PCN-222 (Pt) was further modified by CdS NPs, demonstrating high activity for the HER under both visible and sunlight irradiation (71 645 μmol g_{CdS}^{-1} h^{-1} and 31 326 μmol g_{CdS}^{-1} h^{-1} respectively).[71] The photocatalytic activity was ascribed to the improved photoinduced charge separation due to the presence of both CdS and single Pt atoms, as revealed by PL, PC and EIS measurements. The photocatalytic activity drop (~15%) observed in the fifth consecutive use (5 h per cycle) was attributed to the CdS photocorrosion, the leaching of Cd (21 mg L^{-1}) and Zr (0.017 mg L^{-1}), and the partial decrease of catalyst crystallinity based on PXRD. Regardless of the achieved photocatalytic activity and for the sake of sustainability, it would be recommendable to avoid the use of cadmium element due to its toxicity for humans and the environment.

In another precedent, Hf-PCN-222 containing Pd-metalated porphyrin was further modified with highly dispersed Pt NPs with a mean diameter of 3 nm immobilized within the coordination interspace (3.7 nm) of the PMOF to provide Pt@Hf-PCN-222(Pd) (Fig. 10).[72] Among the various photocatalytic conditions screened, the performance of Pt@Hf-PCN-222(Pd) in the HER was 22 674 μmol g^{-1} h^{-1} under visible light irradiation with a turnover number (TON) value of 4131 after 32 h (TOF: 482 h^{-1}). In addition, the photocatalytic activity was maintained for three consecutive cycles (6 h per cycle) without any decay. The reused solid preserved its features based on XRD, XPS and TEM while 3.5 wt% of the initial Pd leaching occurred. This superior activity of Pt@Hf-PCN-222(Pd) arises from the synergy between dual Pd-porphyrin photosensitizers and Pt NPs as co-catalysts within the confined PMOF network having hydrophilic Hf^{4+}-oxo clusters. Furthermore, Pt@Hf-PCN-222(Pd) showed the highest PC response, thus suggesting its good efficiency in terms of photoinduced charge separation and the occurrence of effective charge transfer from Hf-PCN-222(Pd) to Pt NPs upon illumination with visible light.

Among the different nanostructures, hollow MOFs have shown to be beneficial compared with bulk MOFs due to their high surface area, low density and high mass-diffusion processes.[75] Hence, PCN-222(Zr) MOF hollow nanotubes were synthesized by a competitive coordination method using $ZrCl_4$, TCPP and benzoic acid in an *N*,*N*-dimethylformamide (DMF) and water mixture. Both benzoic acid and water were necessary to achieve the hollow structures built up from the stacking of MOF nanocubes. A series of noble-metal (Ir, Pt, Ru, Au, Pd) single atoms could be successfully immobilized on the MOF through coordination by the porphyrinic core *via* solvothermal post-synthetic modification (Fig. 11).[76] ICP analysis revealed a loading of Ir and Pt of 1.05 and 2.54%, respectively. The photocatalytic performance of the as-prepared solids was tested in the HER using TEOA as a SED under visible-light irradiation. Under the optimized conditions, the pristine MOF showed negligible activity, while the Ir and Pt counterparts exhibited activities of 7.6 μmol g^{-1} h^{-1} and 56.7 μmol g^{-1} h^{-1}, respectively, which clearly indicates the influence of noble single atoms in the targeted reaction. Interestingly, the performance was significantly increased with the MOF containing both Ir and Pt porphyrins to the value of 201.9 μmol g^{-1} h^{-1}, which is about 27 and 3.6 times higher compared with individual Ir or Pt MOFs, respectively. This superior activity was attributed to the synergistic effect from combining Ir-porphyrin photosensitizer and Pt-porphyrin catalyst in a single hollow structure, facilitating a fast mass diffusion. The improved separation of charge carriers, and the reduced charge-transfer resistance were revealed by EIS Nyquist plots.

Ti-MOFs have attracted great attention for photocatalytic applications. Due to the small ionic radius, Ti^{4+} forms strong Ti–O bonds and may present a high coordination number leading to stable MOFs. Moreover, a reversible redox transition between Ti^{4+} and Ti^{3+} under photochemical conditions facilitates effective charge storage.[77] However, the synthesis of crystalline and stable Ti-based MOFs is a true challenge given the high reactivity of Ti^{4+}. Ti-based PMOFs built with the TCPP ligand have been investigated as photocatalysts for the HER.[78,79] In one study, an ultrathin PMOF with Ti-oxo clusters was prepared and tested for the HER.[79] Under optimized conditions, the Ti-based PMOF with Pt cocatalyst provided a hydrogen evolution rate of 8.52 mmol g^{-1} h^{-1} under visible light irradiation. Remarkably, the ultrathin MOF showed nearly 10 times higher activity than the bulk PMOF with Pt, and 4 times higher than the mechanically exfoliated bulk MOF. The photocatalytic activity remained consistent over

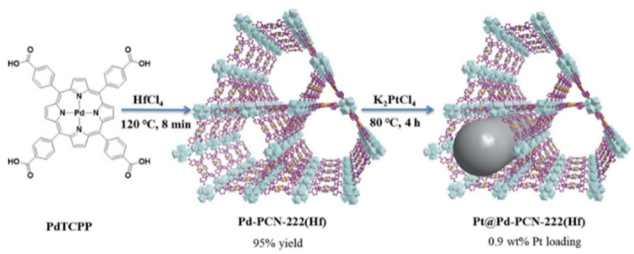

Fig. 10 Synthesis scheme of Pd-PCN-222(Hf) and Pt@Pd-PCN-222(Hf). Reproduced from ref. 72 with permission from *Royal Society of Chemistry*, copyright 2019.

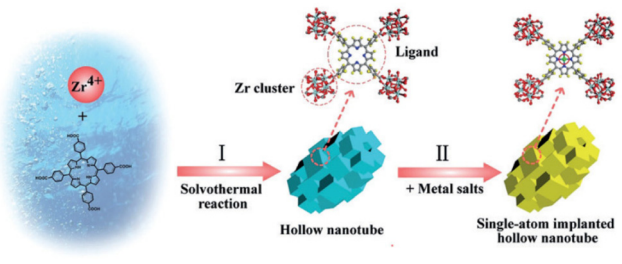

Fig. 11 Synthesis scheme of the hollow nanotube MOFs and immobilization of single-atom within hollow nanotube MOFs. Reproduced from ref. 76 with permission from *Wiley-VCH*, copyright 2018.

three cycles. The enhanced performance was attributed to the efficient photoinduced electron transfer from porphyrin-based ligands (light harvester) to Ti-oxo clusters (catalytic centre), leading to high charge carrier separation. However, given the nearly amorphous nature of the material as evidenced by the PXRD data, the structure–activity relationship cannot be thoroughly addressed.

Ru-based PMOFs have also been reported as efficient photocatalysts for the HER. In that study, two MOFs termed Ru-TBP (TBP: 5,10,15,20-tetra(*p*-benzoic acid)porphyrin) and Ru-TBP (Zn) consisting of Ru^{III} ions arranged in Ru_2 paddlewheel SBUs and TCPP ligands (Fig. 12a) have been synthesized and the HER evaluated.[80] The achieved photocatalytic activity of Ru-TBP and Ru-TBP(Zn) was 0.13 and 0.24 mmol g^{-1} h^{-1}, respectively, and linearly increased as a function of time (up to 98 h). The enhanced HER activity of Ru-TBP(Zn) compared with Ru-TBP is proposed to be due to the better photosensitizing ability of the TBP(Zn) ligand. Interestingly, the TON values achieved after 72 h under visible light irradiation were 21.2 and 39.4 for Ru-TBP and Ru-TBP-Zn, respectively. In contrast, a homogeneous mixture of $Ru^{II}Ru^{III}(CH_3COO)_4(DMF)Cl$ complex with H_4TBP-Zn porphyrin showed a TON value of only 1.4. This superior performance of the MOFs was ascribed to the proximity between the Ru_2 units and the porphyrin ligands in the network (~1.1 nm from Ru to the porphyrin centre), thus facilitating the electron transfer process from excited porphyrins to Ru_2 units (Fig. 12b). The ligand TBP(Zn) is excited to the (TBP-Zn)* state upon visible-light irradiation, from which it can transfer one electron to the Ru_2 SBU to produce $(TBP\text{-}Zn)^+$. Each inorganic SBU first accepts two electrons to form $Ru^{II}Ru^{II}$, and further electron injections to Ru_2 SBU favours the proton reduction to generate H_2. The $(TBP\text{-}Zn)^+$ is reduced back to the TBP-Zn by the TEOA SED to complete the catalytic cycle. The photocatalyst can be effectively reused for six consecutives 1 h cycles, it retains its crystallinity based on PXRD and Ru oxidation state based on X-ray absorption near edge structure (XANES) and exhibits low Ru leaching (0.34 wt%) as evidenced by inductively coupled plasma mass spectrometry (ICP-MS).

Later, DFT calculations were performed to elucidate the enhanced HER activity of Ru-TBP(Zn).[30] These calculations proposed that the molecular connection between the Ru-backbone and the porphyrin plays a favourable role by altering the electronic and optical properties. This leads to improving the efficiency of the photocatalytic activity. Furthermore, computational results revealed a repulsive electron–hole interaction energy, indicating a low rate of electron–hole recombination, which is crucial to achieve electron transfer for the HER, as explained above (Fig. 13).

Table 1 summarizes the results of the selected examples commented on above that represent some of the pioneering, most active and/or stable PMOF photocatalysts for the HER. In addition, other examples that can be found in the literature are included. In general, PMOFs can be used for the development of active photocatalysts for the HER under both visible or solar-light irradiation. Some of the challenges in this area are related to the composition of these photocatalysts, given the need to minimize or even avoid the use of costly noble metals such as Pt and non-sustainable and toxic elements like Cd. Other challenges include the development of more stable porphyrin-based photocatalysts for the HER, assuring longer catalytic performances. Furthermore, it would be highly recommendable to study in more detail the reasons for the decrease of the photocatalytic activity of the materials during the HER. For this purpose, long-term photocatalytic experiments taking place for several weeks or months, even though at the laboratory scale, are still required. In this context, the long-term used photocatalyst should be characterized by a combination of characterization techniques including at least the same as those employed for the characterization of the fresh material, like PXRD, XRD, TGA, SEM and TEM, among others.

Photocatalytic HER using PMOF composites

In analogy to the area of inorganic semiconductors,[81–83] an important advancement in the field of MOFs, and in particular PMOFs,[84,85] lies in the development of heterojunctions to

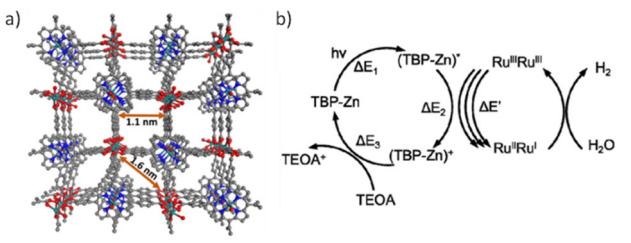

Fig. 12 (a) Perspective view of the Ru-TBP crystal structure down the (100) direction. (b) Proposed catalytic cycle for visible-light-driven hydrogen evolution catalysed by Ru-TBP(Zn). Reproduced from ref. 80 with permission from the *American Chemical Society*, copyright 2018.

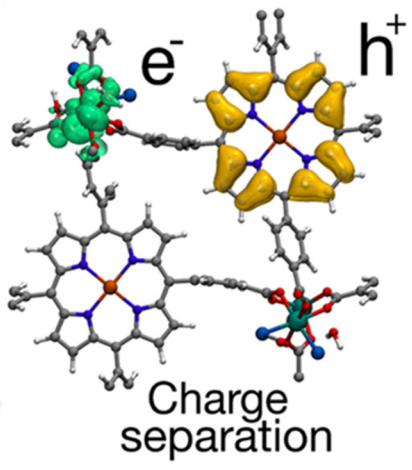

Fig. 13 Representation of the electron (green) and hole (orange) densities in the charge-separated state of the Ru-TBP(Zn) MOF. Reproduced from ref. 30 with permission from *American Chemical Society*, copyright 2020.

further increase their catalytic activity. A heterojunction consists of an interface contact between two semiconductors characterized by a different energy level band diagram that allows photoinduced charge carrier migration between the two solids. This strategy aims to increase the photocatalytic efficiency by spatially separating the electrons and the holes in a way that their recombination is, at least, partially restricted. The fundamentals of heterojunctions can be found elsewhere.[82,83]

In this context, several heterojunctions using PMOFs with other inorganic materials like TiO_2,[86] titanate nanotubes (TNTs),[87] $ZnIn_2S_4$,[88] Nb_6O_{17},[89] and CdS[90] and recently using metal-free materials such as carbon nitrides[84,85] and covalent-organic frameworks (COFs)[91,92] were reported. Table 2 summarizes the results in terms of photocatalytic activity/stability. Regardless of the good photocatalytic activity achieved in most reports, in some cases this activity and/or photocatalyst stability decreases in large extent or has not been addressed. In recent years, a couple of studies have been reported on the development of 2D/2D heterojunctions based on PMOFs and carbon nitride (CN)-based materials for the HER.[84,85] One of the intrinsic properties of these 2D/2D heterojunctions is to facilitate the interface contact between the counterparts and, thus, the photocatalytic activity. Similarly, some studies have described the possibility of preparing MOF/COF composite photocatalysts. Metal-free COFs often exhibit fast electron–hole recombination;[91] thus combining them with MOFs has been reported as a potential strategy to favour charge separation and increase the efficiency of the photocatalytic process, including water splitting. For a comprehensive description of the merits and challenges in using MOFs, COFs and their composites as photocatalysts, the reader is referred to the recent reviews.[91,93]

CN-based materials are a series of layered and porous metal-free and medium-band gap semiconductors that have found application as photocatalysts for environmental applications and to produce solar fuels, among others.[94,95] In this context, a recent work has reported the development of a novel 2D/2D heterostructure consisting of P-doped CN nanosheets with Zn-PMOF by adopting an electrostatic self-assembly. The photocatalytic performance of this composite was studied in the HER.[84] TEM images (Fig. 14i) of the P-doped CN/Zn-$PMOF_{1.5}$ hybrid structure showed several regularly shaped Zn-PMOF nanosheets (sizes of 20–50 nm) randomly distributed

Table 2 Summary of selected examples using PMOF heterojunctions as photocatalysts for the HER

Photocatalyst	Reaction conditions	Activity	General remarks	Ref., year
Pt/Cu-TCPP PMOF on TiO_2 microspheres	Photocatalyst (10 mg), H_2O (50 mL), TEOA (10 mL), UV-Vis irradiation (Xe lamp, 340 to 780 nm), 6 h	86.11 mmol g^{-1}, 6 h irradiation	The photocatalyst activity decreases up to 84.8% after 5 cycles (6 h per cycle). The reused sample exhibits some changes in the UV-Vis spectrum (other characterization was not conducted) Stability of the composite improved compared with its counterparts	86, 2022
TNTs/Co-TCPP MOF	Photocatalyst (10 mg), H_2O (50 mL), TEOA (10 mL), UV-Vis irradiation (300 W Xe lamp), 6 h	5.8 mmol g^{-1}	The photoactivity drops in the second use about 70% and, then, is maintained up to the fourth use (6 h per cycle). The reused solid exhibits some changes based on UV-Vis diffuse reflectance spectra, XPS and SEM analyses	87, 2023
$ZnIn_2S_4$@PCN-224	Photocatalyst (50 mg), H_2O aqueous solution (100 mL; 0.35 M $Na_2S{\cdot}9H_2O$ and 0.25 M Na_2SO_3), visible light source (300 W lamp, $\lambda > 420$ nm cut off), 5 h	0.284 mmol h^{-1}	AQY of 6.45% at 420 nm; photocatalyst was reused for 5 times (5 h per cycle) maintaining the H_2 production while characterization of the solid after use has not been addressed	88, 2021
Co-TCPP PMOF on Nb_6O_{17} microflowers	Photocatalyst (10 mg), H_2O (50 mL), TEOA (10 mL), Xe lamp (300 W), 5.5 °C, 6 h	81 μmol	The sample can be reused five times (6 h per cycle) and a slight increase of activity was observed upon reuse. The reused solid exhibits some changes based on SEM, XPS and UV-Vis (XRD not shown). Stability of the composite improved compared with its counterparts, accumulated TON of 53	89, 2022
Pt@CdS NPs/2D Zn-TCPP	Photocatalyst (20 mg), H_2O aqueous solution (50 mL; 0.25 M Na_2S and 0.35 M Na_2SO_3), visible light source (300 W lamp, $\lambda > 420$ nm filter), 5 h	15.3 mmol g^{-1} h^{-1}	Photocatalyst stability and reusability have not been addressed. Type II heterojunction	90, 2022
B-doped-CN@Co-PMOF	Photocatalyst (5 mg), H_2O solution (25 mL; 700 mg ascorbic acid), H_2PtCl_6 solution (0.8 wt%), irradiation source (Xe lamp 225 W, CEL-PF300-T8), 6 °C, 3 h	33.17 mmol g^{-1} h^{-1}	Most of the photocatalytic activity (>90%) is retained during the four uses (3 h per cycle) while the reused solid was not characterized	85, 2022
P-doped CN/Zn-PMOF	Photocatalyst (5 mg), H_2O (25 mL), H_2PtCl_6 solution (0.8 wt%), ascorbic acid (800 mg), irradiation source (Xe lamp, 225 W, CEL-PF300-T8), 6 °C, 3 h	65.3 mmol g^{-1} h^{-1}	The photocatalyst is stable and reusable for 5 consecutive uses	84, 2022

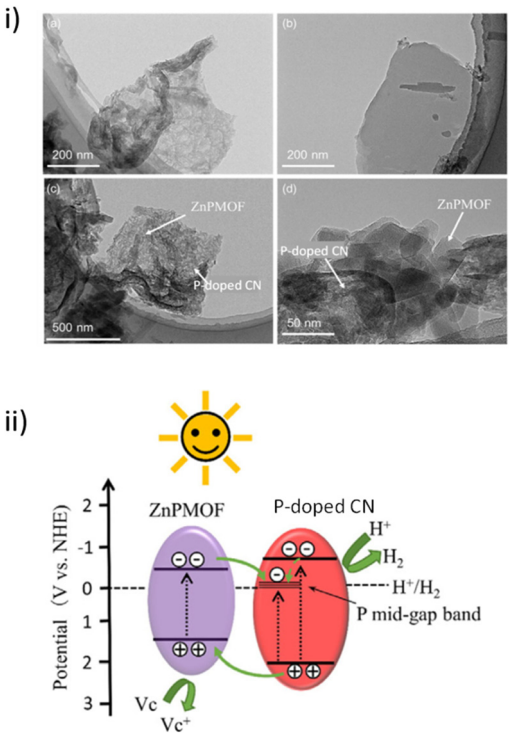

Fig. 14 (i) TEM images of (a) P-doped CN, (b) Zn-PMOF, and (c) and (d) P-doped CN/Zn-PMOF$_{1.5}$. (ii) Schematic diagram of electron and hole migration between P-doped CN and Zn-PMOF. Reproduced from ref. 84 with permission from *Wiley-VCH*, copyright 2022.

over the edge sides of the P-doped CN (size ~ 120 nm). The P-doped CN/Zn-PMOF photocatalyst afforded a H_2 evolution rate of 65.3 mmol g^{-1} h^{-1} under simulated solar irradiation using ascorbic acid as a SED, 2.2 and 49.1 times higher compared with P-doped CN and Zn-PMOF alone, respectively. This superior performance of P-doped CN/Zn-PMOF was attributed to its unique 2D/2D heterostructure that results in a more efficient photoinduced charge separation. The Nyquist curve radii of the P-doped CN/Zn-PMOF were smaller compared with both the P-doped CN and Zn-PMOF, thus clearly showing the formation of the intimate interfacial contact between P-doped CN and Zn-PMOF that can efficiently reduce the charge carrier migration resistance. Furthermore, phosphorous doping endows CN with enhanced separation sites of photoinduced charge carriers and consequently establishes Type II heterojunctions with Zn-PMOF. In a typical mechanism, both Zn-PMOF and P-doped CN are excited by generating electron–hole pairs under the simulated sunlight irradiation. Then, the photoinduced electrons migrate from the LUCO energy of the Zn-PMOF to the conduction band of the P-doped CN, while holes migrate from the valence band of the P-doped CN to the HOCO energy of the Zn-PMOF (Fig. 14ii). The solid was recycled for five cycles (3 h per cycle) with no decrease in its photocatalytic activity.

In a related work, a series of acidified B-doped CN and Co-PMOF composites has been prepared *via* ultrasonication followed by magnetic stirring of at 80 °C for 10 h according to Fig. 15.[85] The formation of the self-assembly 2D/2D composite was confirmed by TEM and energy dispersive X-ray (EDX) analyses. The materials were used as photocatalysts for the HER in the presence of H_2PtCl_6 (0.8 wt%; Table 2) and ascorbic acid as a sacrificial agent. An optimized composite exhibited a photocatalytic activity (33.17 mmol g^{-1} h^{-1}) which is about 3 and 100 times higher than the sole B-doped CN and Co-PMOF, respectively. This activity increase was associated with a better photoinduced charge separation and lower charge resistance migration of the composites *vs.* the counterparts, as revealed by PC and ESI measurements. From the experimentally estimated energy band level of the Co-PMOF and B-doped CN, the contribution of DFT calculations and the observed photogeneration of hydroxyl radicals in water, it was proposed that the composite under illumination operates under a Z-scheme mechanism, as illustrated in Fig. 15.

Photocatalytic OWS

Most of the studies using MOFs and PMOFs as photocatalysts for water splitting have primarily focused on the HER with the aid of sacrificial agents.[42,56–62] Regardless of the excellent advancements in the field, the use of a SED such as MeOH or TEOA for the photocatalytic HER hampers the real applications. Alternatively, some studies have reported the possibility of using biomass wastes as sustainable feedstocks for this purpose.[97] Nevertheless, similar to the progress achieved using inorganic semiconductors in large-scale practical applications,[50] the next major advancement entails the development of efficient MOF-based photocatalysts capable of solar-driven, sacrificial agent-free OWS into H_2 and O_2.[24] Furthermore, the field of OWS by employing MOFs as photocatalysts has recently been attractive due to their tuneable active sites, and well-defined structure with high surface area. The reader is referred to the recent reviews in this field for an in-depth understanding on the challenges of using MOFs as photocatalysts for OWS, solar fuel production and advanced characterization techniques.[39,46,65]

In this context, a pioneering study reported in 2017 the use of Ni^{2+} ions coordinated to the amino groups of MIL-53(Al)-NH_2 material for this purpose.[98] Since then, the majority of studies have focused on the development of MOF-based photocatalysts as single components like MIL-125(Ti),[99,100] UiO-66 (Zr),[101,102] and squarate-based IEF-11(Ti),[103] among others.[104] Some of the strategies developed to expand the visible light absorption include the use of electron donor functional groups in the aromatic rings of the 1,4-benzene dicarboxylate (bdc) organic ligand. For example, this has been employed in the case of MIL-125(Ti)-NH_2 or UiO-66(Zr)-NH_2 photocatalysts, allowing an expansion of the absorption up to about 450 nm. Other investigations focused on expanding the visible-light absorption of UiO-66(Zr) by replacing Zr^{4+} by Ce^{4+} ions in the metal nodes.[54,105] Furthermore, the preparation of mixed-metal UiO-66(Zr/Ti), UiO-66(Zr/Ce) or the trimetallic UiO-66 (Zr/Ce/Ti) has proved to be an appropriate strategy to boost the photocatalytic OWS under visible light irradiation.[101,106] More recently, the development and use of MOF-on-MOF composites

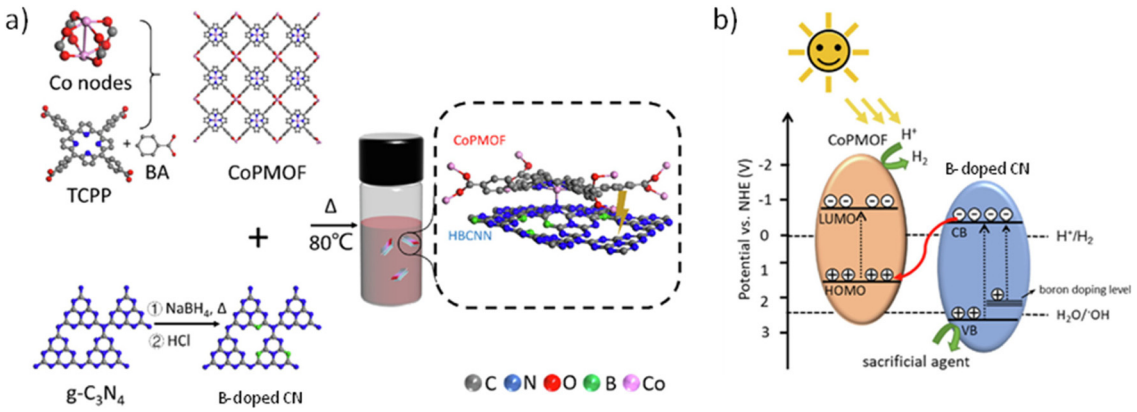

Fig. 15 (a) Synthesis illustration of B-doped CN/Co-PMOF. (b) Proposed Z-scheme heterojunction between B-doped CN and Co-PMOF. Reproduced from ref. 85 with permission from the *Elsevier*, copyright 2022.

with UiO-66 materials has been reported for the first time to improve the activity of the counterparts toward photocatalytic OWS under simulated sunlight irradiation.[107]

Despite the efforts to increase visible light absorption and consequently improve the efficiencies of solar-driven OWS, most of these photocatalysts are limited by an absorption onset around 500 nm. To overcome these limitations, several investigations have explored the use of PMOFs for OWS.

PMOFs and PMOF-composites for photocatalytic OWS

In the seminal contribution, the integration of two types of MOFs nanosheets – a HER-MOF and a water oxidation reaction (WOR)-MOF in a liposome structure – was adapted as a strategy to separate the generated charges and related half-reactions for the OWS.[53] The integrated HER-MOF nanosheets are based on Hf_6 clusters and metalloporphyrins with the chemical composition: $[Hf_6(\mu_3\text{-}O)_4(\mu_3\text{-}OH)_4(\mu_1\text{-}OH)_2(\mu_1\text{-}H_2O)_2(HCO_2)_6[(TCPP)Zn]_{1-x}[(TCPP)Pt]_x]$. In its structure two types of metalloporphyrin are present, the light-harvesting Zn-porphyrin and catalytic Pt-porphyrin. The solid was functionalized by hydrophobic pentafluoropropionic acid groups on the inorganic SBU to facilitate its incorporation into the lipid bilayer of a liposome (Fig. 16). On the other hand, the WOR-MOF flakes are built up from $[Zr_{12}(\mu_3\text{-}O)_8(\mu_3\text{-}OH)_8(\mu_2\text{-}OH)_6]$ SBU and [Ru^{II}(2,2′-bipyridine)$_2$(2,2′-bipyridine-5,5′-dicarboxylic acid)] metalloligands that act as photosensitizers and Ir-bipyridine complexes are introduced in the MOF structure to act as catalytic sites. The WOR-MOF nanosheets are localized in the hydrophilic part of the liposome. This integrated liposome–MOF assembly exhibited OWS under photocatalytic conditions with an AQY of 1.5 ± 1%. This efficiency was attributed to the ultrafast electron transport from (Zn-porphyrin and $[Ru(2,2'\text{-bipyridine})_3]^{2+}$) to the reaction sites (Pt-porphyrin and Ir-bipyridine) in the MOFs and efficient charge separation in the lipid bilayers.

In another example, Garcia and coworkers reported the influence of transition metal ions within the porphyrin-based PCN-222 over the simulated sunlight-driven OWS.[108] Under

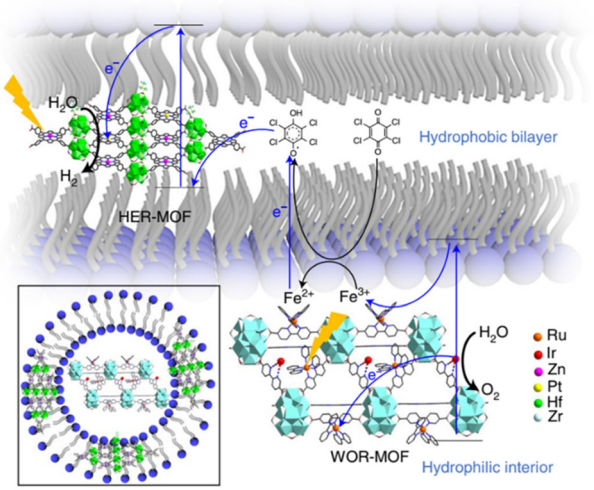

Fig. 16 Structure of the liposome-MOF for OWS and the proposed 'Z-scheme' electron-transfer chain in the liposome-MOF system. Reproduced from ref. 53 with permission from Springer *Nature*, copyright 2021.

the optimized photocatalytic conditions, Zr-PCN-222(Zn) showed HER efficiency around 1.5 mmol of H_2 per gram of photocatalyst with MeOH, which is corresponding to an HER rate of 65.8 μmol g^{-1} h^{-1}. On the other hand, Zr-PCN-222(Fe) afforded the total accumulated H_2 and O_2 rate of 904 μmol g^{-1} and 275 μmol g^{-1}, respectively, after 110 h. However, a clear decay in the OWS activity was observed upon five cycles and was ascribed to a partial leaching of Zr and a significant decrease of the surface area. Additionally, TAS measurements indicated the formation of a charge-separated state and the oxidation of water taking place on the positive holes within the microsecond timeframe. Importantly, this study demonstrates the achievement of noble-metal-free, PMOFs as photocatalysts for sustainable OWS.

More recently, some of us reported the one-pot synthesis of a mixed-metal MIL-173(Ti/Zr) phenolate PMOF and its appli-

cation as a photocatalyst for OWS under simulated sunlight irradiation (Fig. 17).[109] Experimental characterization data together with a computational approach revealed the location of the HOCO in the porphyrin-based ligand, while the presence of Ti atoms contributes to the LUCO of the material and decreases the band gap with respect to the parent MIL-173(Zr). An optimized MIL-173(Zr/Ti)-40 having 40 mol% of titanium inside the inorganic SBU exhibited the highest photocatalytic activity of the series. The photocatalytic H_2O oxidation by MIL-173(Zr/Ti)-40 was confirmed using labelled $H_2{}^{18}O$, evidencing the formation of $^{18}O_2$ *via* gas chromatography-mass spectrometry (GC-MS) analysis. The enhanced photocatalytic activity observed in the case of the mixed-metal MIL-173(Zr/Ti)-40 sample compared with the analogs with lower Ti content was attributed to its superior photoinduced charge separation efficiency, as revealed by PC and PL measurements. Table 3 summarizes the selected examples commented above that use PMOFs as photocatalysts for OWS.

In summary, PMOFs are among the most active MOF-based materials for both the HER and OWS under visible or sunlight irradiation. This can be primarily attributed to their superior light absorption properties, enabling the capture of a significant part of the visible light compared with non-porphyrin-based MOFs, typically limited to absorption up to 450 nm. In addition, incorporation of Pt through the metalation of the porphyrin ligand is a unique strategy that has proved to be more efficient in achieving high catalytic activities compared with the use of Pt NPs. In general, PMOFs constructed from high-valence ions, such as Al^{3+}, Zr^{4+} and Ti^{4+}, are needed to meet the requirements for the development of stable photocatalysts in water.

Considering the high tunability of PMOFs in terms of organic ligand modification acting as photosensitizers, the possibility to prepare mixed-metal materials that favour the photoinduced charge separation and the deposition of single metals as co-catalysts, a further expansion of this field is expected. Besides, as several examples have now shown the possibility to achieve PMOF composites with other photoactive materials such as carbon nitrides, these assemblies can further promote the activities for OWS.

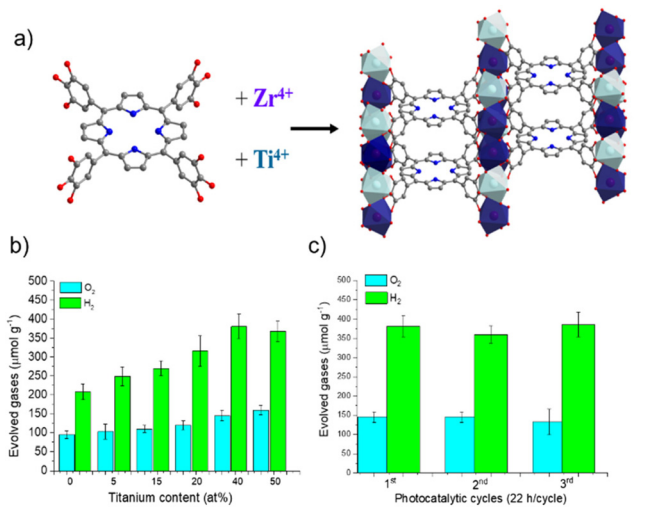

Fig. 17 (a) Synthesis scheme for the mixed metal MIL-173(Ti/Zr), (b) photocatalytic OWS under simulated sunlight irradiation using MIL-173 (Zr) and MIL-173(Ti/Zr) solids having different Ti at% contents, and (c) photocatalytic stability upon 3 cycles. Reproduced from ref. 109 with permission from the *Royal Society of Chemistry*, copyright 2022.

C. Water remediation

Clean freshwater is a prerequisite for life and its availability is essential for supporting sustainable development in areas such as energy, food production and healthy ecosystems. Nevertheless, its supply is not secured for a growing part of the population. During the last decades, increasing contamination in water sources has led to the deterioration of water quality, endangering health and progress. Human activities like the overuse of agrochemicals, improper disposal of wastes, leakage of septic tanks, or simply the lack of tertiary or quaternary treatments of wastewater have led to the introduction of emerging organic contaminants (EOCs) in the aquatic environment. EOCs are newly detected organic pollutants, including pharmaceuticals, personal care products, agrochemicals, and industrial compounds, presenting a serious concern due to their toxic effects and potential bioaccumulation in the food chain.[111] Recently, the European Union (EU) Drinking Water Directive set general drinking water quality standards for some EOCs.[112] For instance, the summed concentrations of pesticides and their metabolites should be under 0.5 μg L^{-1}. However, approximately 80% of the total reported analysed pesticides concentrations were much higher than the EU water quality standards (*e.g.* 40, 25 and 20-fold higher concentration of amitrole, diuron and terbuthylazine herbicides in the Arc river, France, respectively).[113]

Despite conventional wastewater treatment, EOCs elimination remains insufficient, necessitating a development of alternative more effective methods. In recent years, the scientific and industrial community has studied new processes to eliminate EOCs from water (*i.e.* chlorination,[114] sonodegradation,[115] inorganic heterogeneous catalysis[116]). Among these technologies, MOFs have also gained attention due to their high tunability and porosity. First, archetypal MOFs like MIL-53(Cr) and MIL-101(Cr) were reported in the adsorptive removal of methyl orange (MO) dye,[117] or MOF-5 in the catalytic degradation of an industrial product (phenol).[118] As the implementation of MOFs based on photoactive molecules is particularly well suited to this topic, PMOFs have been studied as potential water remediation materials for EOCs removal since 2017.

In order to provide a comprehensive overview and compare the activity of each material, the composition and properties of each PMOF or PMOF-based composite are presented in this review. However, comparing the materials' performances from the published studies poses challenges due to varying testing conditions (*e.g.* concentration of contaminant and PMOF,

Table 3 Summary of selected examples using PMOFs as photocatalysts for OWS

Photocatalyst	Reaction conditions	Activity	General remarks	Ref., year
Liposome-based MOF Pt-porphyrin and Ir-bipyridine	Photocatalyst suspension, redox relays (tetrachlorobenzoquinone/tetrachlorobenzohydrosemiquinone), and (Fe^{3+}/Fe^{2+}), H_2O (20 mL), light source 400 nm LED + 450 nm light emitting dioide (LED), 72 h	836 and 418 μmol g^{-1} for H_2 and O_2, respectively, after 72 h	AQY 1.5 ± 1% at 436 nm	53, 2021
Zr-PCN-222(Fe)	Photocatalyst (20 mg), Milli-Q water (20 mL), solar simulator (1 Sun), 1.5 G filter, 22 h	904 and 275 μmol g^{-1}, for H_2 and O_2 respectively, after 110 h	—	110, 2022
MIL-173(Zr/Ti)-40	Photocatalyst (10 mg), H_2O (20 mL), simulated sunlight irradiation (Xe–Hg lamp 150 W, 1.5 AM filter), 35 °C, 22 h	381 and 145 μmol g^{-1} for H_2 and O_2, respectively, after 22 h	AQY 0.11% at 450 nm	109, 2022

irradiation power, water source, a single contaminant or a mixture of contaminants). It is also important to note that reproducibility challenges exist in MOF synthesis.[119] This can lead to significant variability in S_{BET} values when the same material is prepared by different research groups (as can be observed in the tables below). This can be related to the presence and number of defects in the PMOFs, their purity or the activation procedures used. Moreover, in a number of reports, an initial adsorption step is employed to reach the contaminant adsorption/desorption equilibrium within the MOF; however, information on the sorption kinetics and EOCs adsorption capacities is often omitted. Considering the ultimate goal of applying these materials in continuous flow water treatment plants, where adsorption and photodegradation will occur concurrently, studies performing simultaneous adsorption and photodegradation processes will be better suited for practical implementation. Furthermore, the addition of co-reactants (oxidants, scavengers) to achieve the EOCs' degradation hampers their real application in water treatment.

To facilitate the comparisons, we normalize the pollutant degradation activities to the quantity of removed pollutant (μg) per catalyst amount (mg^{-1}) per reaction time (h^{-1}) (the normalized values are underlined in the text), assuming the limitations stated above. PMOFs have been proposed for the removal of a wide range of contaminants, including dyes, pharmaceuticals, and bisphenol compounds (see some examples in Fig. 18). This review categorizes the best-performing PMOFs as a function of the EOCs' origin. Additionally, the removal of toxic metals and bacteria from water using PMOFs is briefly discussed in the final section.

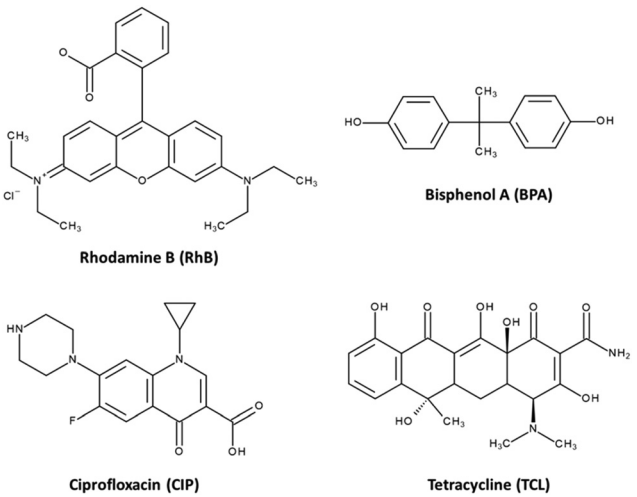

Fig. 18 Chemical structures of the most studied EOCs eliminated from water by PMOFs.

Dyes

Textile production is estimated to be responsible for about 20% of global clean water pollution from dyeing and finishing products.[120] Particularly, wastewater discharges from textile industries are highly coloured, containing several highly toxic dyes and their breakdown products. This is particularly worrying considering that clothing production doubled from 2000 to 2015. Aside from this, dyes have been classically used as model molecules in water decontamination experiments for the ease of monitoring of their degradation by spectroscopic techniques. In 2017, the first report described the efficient photocatalytic performance of a 3D PMOF PCN-222(Zn) (see the introduction and Fig. 1a for the material description). PCN-222(Zn) is based on the Zn metalated ligand and was studied for the degradation of rhodamine B (RhB) dye under simulated sunlight conditions (Fig. 19).[121] In a way to enhance the photocatalytic properties of the material, TiO_2 NPs were incorporated into the PCN-222(Zn) structure, leading to a

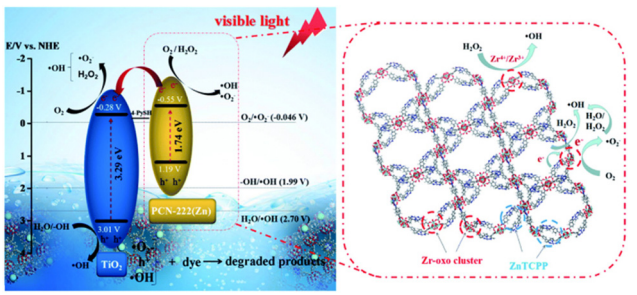

Fig. 19 Schematic diagram of the possible visible-light-driven photocatalytic degradation mechanism toward the TP-222(Zn) composite with the integration of TiO_2 NPs into PCN-222(Zn). Reproduced from ref. 121 with permission from the *Royal Society of Chemistry*, copyright 2017.

TP-222(Zn) composite presenting relevant properties for water remediation, such as high porosity (S_{BET} = 1400 m^2 g^{-1}; pore size ≈ 13 & 37 Å), chemical stability and absorption in the visible light region. The TiO_2 NPs serve as electron acceptors, generating a charge transfer that would *a priori* promote electron–hole pair formation and, therefore, improve the photocatalytic activity of the composite. In this study, a separation of the adsorption and degradation steps was adopted: 40% of the overall RhB was first adsorbed within the material in order to enhance the subsequent photocatalysis due to the pollutant proximity to the MOF active centres. The TP-222(Zn) composite was able to fully degrade the RhB in water, and after 270 min under irradiation, the dye degradation reached values 2.1 times greater than the ones obtained for the pristine PCN-222 (Zn). Regarding the proposed photodegradation mechanism (Fig. 19), the presence of TiO_2 NPs is necessary to significantly improve the charge-separation efficiency, as demonstrated by time-resolved photoluminescence (TRPL) and EIS. The active species involved in the RhB photocatalytic degradation were identified *via* the use of different scavengers. For instance, N_2 drastically inhibited the RhB degradation, indicating the major degrader role of the $^{\bullet}O_2^-$ radical, whereas the effect of $HO^{\bullet}$ radical was evidenced in the presence of H_2O_2 and isopropanol (IPA) as scavenger. In terms of recyclability, the photocatalyst was active during 4 consecutive cycles, with only 1.7% of TiO_2 leaching, demonstrating its stability under the working conditions (Table 4). In addition, the almost unchanged XRD patterns and SEM images of TP-222(Zn) after the recyclability studies confirmed the structural stability and the high dispersion of the TiO_2 NPs after catalytic tests.

From this initial work, dyes degradation remained an important topic for EOCs photodegradation by PMOFs and related composites. Interestingly, RhB is the most studied molecule, and is found in 7 over the 9 dye-dedicated articles. For this reason, RhB is used in this section to compare the photocatalytic efficiency of different PMOFs. When comparing 2D and 3D materials (Table 4), a generally superior pollutant removal in 3D materials is observed, probably as a result of the higher accessible porosity in these structures. Furthermore, the lack of information regarding the dyes adsorption process (adsorbed amount, time to reach the equilibrium, *etc.*) hampers a detailed comparative revision of the photocatalytic performance of each material. Another challenge in comparing dyes elimination using PMOFs is the implementation of various additional techniques to enhance degradation, such as the ultrasound in the elimination of MO by (2D) Zn-TCPP MOF,[122] or the possible simultaneous adsorption/photodegradation of the RhB, methylene blue (MB) and Congo red (CR) in 2D Cu-TCPP MOF.[123] Taking into account the normalized values (Table 4), it can be observed that PMOF-based composites present overall a better catalytic efficiency than their single PMOF counterparts. These composites are mainly formed by combining the PMOF with semiconductors, like TiO_2,[121] Fe_2O_3,[124] ZnO[125] or In_2O_3,[126] and in all cases the improved activity is ascribed to the favourable charge transfer capability.[127,128]

That is the case of two PCN-222 nanocomposites: Fe_3O_4@SiO_2@PCN-222(Fe),[129] and 2N-CDs@PCN-222@PNIPAM[130] based on the iron and free-base porphyrin respectively. These composites are prepared by direct synthesis of the MOFs in media containing Fe_3O_4@SiO_2 magnetic microspheres or carbon dots (CDs), respectively. In the latter case, a further modification of the material's surface with a catechol-terminated thermo-responsive poly(*N*-isopropylacrylamide) (PNIPAM) having various chain lengths is performed. The two composites display very different porosities with the S_{BET} being significantly higher for Fe_3O_4@SiO_2@PCN-222(Fe) than for 2N-CDs@PCN-222@PNIPAM (S_{BET} = 2000 *vs.* 288 m^2 g^{-1}, respectively). This is probably due to the presence of the PNIPAM polymer in the second composite strongly reducing the accessible porosity. An RhB adsorption step was implemented in both cases, after which photodegradation values of 552 and 474 μg mg^{-1} h^{-1} were obtained with Fe_3O_4@SiO_2@PCN-222(Fe) and 2N-CDs@PCN-222@PNIPAM, respectively. Considering the photocatalytic reaction, Fe_3O_4@SiO_2@PCN-222(Fe) was irradiated with a higher intensity than 2N-CDs@PCN-222@PNIPAM (500 *vs.* 300 W) and without a cut-off filter (including both the UV and visible ranges), and that could also account for its better photocatalytic performance. Furthermore, Fe_3O_4@SiO_2@PCN-222 (Fe) was able to remove, even at higher percentages, the erythrosine B (EryB) and Rose Bengal (RoseB) dyes with 99 and 98% elimination rates after 2 h irradiation, corresponding to 594 and 588 μg mg^{-1} h^{-1}, respectively. The degradation mechanism was studied through the addition of different scavengers and highlighted the predominance of the superoxide radical ($^{\bullet}O_2^-$) in the pollutants' photodegradation. Both composite materials were demonstrated to be catalytically active after 3 and 5 consecutive cycles, respectively, maintaining their crystalline structure along all the experiments, as evidenced by PXRD.

A related study described the synthesis of a capsule-like bimetallic Hf-PCN-222(Ni) where Hf^{4+} is part of the inorganic SBU, while Ni^{2+} ions are bonded to the N inside the porphyrin rings, and the free-base counterpart Hf-PCN-222.[131] Authors described the simultaneous removal of four dyes using Hf-PCN-222 where the porphyrin is in its free base form, using visible light (Xe lamp 300 W) in only 2 h, reaching degradation percentages of 99.7% for RhB (40% adsorption/desorption equilibrium, 2 h), 98.6% for basic violet 14 (BV14, 87%), 55.5% for crystal violet (CV, 30%), and 67.9% for acid black 210 (AB210, 27%). The removal efficiencies increased for the metalated form of the MOF, Hf-PCN-222(Ni) reaching degradation percentages of 100% for RhB (99% adsorption/desorption equilibrium, 2 h) and BV14 (87%), 70% for CV (60%) and 83% for AB210 (47%). These differences in the total removal percentages may be related to the higher surface area of the Ni-metalated MOF (S_{BET} = 2000 *vs.* 1010 m^2 g^{-1}). The superior surface area for the latter does not seem intuitive considering its higher density, and the authors argue that the co-existence of Ni^{2+} and Hf^{4+} prominently increases the pore size (from

Table 4 PMOFs for dyes photocatalytic degradation

	PMOFs	Metal	S_{BET} (m^2 g^{-1})	Photosource	Dye; concentration (mg L^{-1}); volume (mL)	Catalyst amount (mg)	Degradation; initial adsorption (%)	Normalized activity[a] (μg pollutant removed mg^{-1} catalyst h^{-1})	Adsorption time; irradiation time (h)	Number of cycles	Ref., year
2D-PMOFs	(2D) Cu-TCPP	Cu	343	300 W Xe lamp $\lambda \geq 420$ nm	RhB; 20; 100 MB; 100; 100 CR; 40; 100	5	82; NM 63; NM 89; NM	54 210 118	6; 2	NM	123, 2020
	(2D) Zn-TCPP	Zn	854	Sun power (100 Mw cm^{-2})	MO; 10; 10	2	46.2; NM	287	1; NM	5	122, 2022
3D-PMOFs	TP-222(Zn)	Zr	1400	500 W Xe lamp $\lambda \geq 420$ nm	RhB; 50; 50	2.4	100; 40	231	4.5; 2.5	4	121, 2017
	Hf-PCN-222	Hf	1010	Xe lamp	RhB, BV14, CV & AB210; 50; 150	15	99; 40 98; 87 55; 30 68; 27	125 122 68 85	2; 2	3	131, 2021
	Hf-PCN-222(Ni)	Ni/Hf	2000	$\lambda \geq 420$ nm			100; 99 100; 87 70; 60 83; 47	125 125 87 103			
Composites	Fe_3O_4@SiO_2@PCN-222(Fe)	Zr	2000	500 W Halogen lamp	RhB, EryB or RoseB; 100; 30	10	92; NM 99; NM 98; NM	552 594 588	2; 1	3	129, 2021
	2N-CDs@PCN-222@PNIPAM	Zr	288	300 W Xe lamp $\lambda \geq 420$ nm	RhB; 20; 100	50	98; NM	474	0.08; 0.5	5	130, 2021
	Ag@MOF-525	Zr	2250	500 W Xe lamp $\lambda \geq 420$ nm	RhB; 20; 50	50	91; NM	18	1; 1	4	134, 2023
	Nmlm (PCN-222 + NU-100)	Zr	2300	150 W halogen lamp $370 < \lambda < 800$ nm	RhB; 50; 50	5	95; NM	118	4; 8	3	133, 2020
	PCN-224/TA/PVDF	Zr	Membrane	Xe lamp Simulated sunlight	MB; 10; 50	100	96; 18	5	1; 1	NM	132, 2021

AB210: acid black 210; BV14: basic violet 14; CR: Congo red; CV: crystal violet; EryB: erythrosine B; MB: methylene blue; MO: methyl orange; RhB: rhodamine B; Rose B: Rose Bengal B. NM: Not mentioned. [a] Normalized activity: normalized data calculated by μg removed pollutant per mg catalyst per h.

2.5 nm in Hf-PCN-222, to 2.26 nm in Hf-PCH-222(Ni)) and gives a more uniform pore distribution. Regarding the photocatalytic degradation mechanism, the use of *p*-benzoquinone (*p*-BQ) scavenger in the RhB degradation experiments confirmed that superoxide radicals are the main reactive species when using Hf-PCN-222. In contrast, with Hf-PCN-222(Ni) as the photocatalyst, the addition of ammonium oxalate demonstrated that the holes (h^+) were the major reactive species. Finally, the cyclability of the materials was tested only using RhB dye instead of the mixture of contaminants. Hf-PCN-222 (Ni) was demonstrated to be efficient (up to 90.6% of RhB elimination after 3 cycles) and structurally stable (PXRD) after 3 consecutive RhB removal cycles while the non-metalated MOF lost its crystallinity and its catalytical activity considerably decreased in the third cycle. No information is provided regarding the recyclability of the material in a mixture of contaminants.

As most MOFs are generally in powder form, they are difficult to recover and recycle from the solution, and this limits their real application in water remediation. Recently, a membrane based on the composite material formed from PCN-224, tannic acid and polyvinylidene fluoride (PCN-224/TA/PVDF) was fabricated *via* an *in situ* deposition method, allowing the anchoring of PCN-224 NPs on the surface. The membrane was tested for oil-in-water separation and MB/RhB adsorption/photocatalytic degradation.[132] This membrane exhibits a high separation efficiency of above 99% for a series of oil-in-water emulsions, as well as adsorption efficiencies above 98.5 and 99.4% for MB and RhB in the concentration range of 10 to 50 ppm, respectively. Under a 300 W Xe lamp irradiation, a degradation rate of 95.6% for MB was observed in 60 minutes, and no significant decrease in photocatalytic activity was found after five cycles. Further tests developed using 1,3-diphenylbenzofuran (DPBF) as scavenger demonstrated the $^1O_2$ photogeneration capacity of the membrane, singlet oxygen being the main active species in the dye photodegradation reactions. The membrane exhibited good renewability and reusability, being a promising material for application in wastewater remediation; however no information regarding MOF stability within the membrane is provided.

Eventually, a Zr-based, nanosized mixed-ligand MOF (nMLM) composed of porphyrin and pyrene derived ligands was reported by Lee *et al.*[133] Although not clearly specified, the MOF structure was claimed to be close to the ones of PCN-222 and NU-1000, which are MOFs based on the TCPP and pyrene tetracarboxylate ligands, respectively. The ratio of porphyrin to pyrene ligands was 27% as deduced from liquid nuclear magnetic resonance (NMR) of the digested MOF sample. nMLM displays a large surface area of around 2310 $m^2\ g^{-1}$, and its photocatalytic performance in the photodegradation of RhB in the presence of hydrogen peroxide as oxidant was assessed. The reaction rate constant of 0.01117 min^{-1} was determined for nMLM, which is about 2.9 and 2.5 times greater than those of PCN-222 and NU-1000, respectively. Furthermore, through trapping experiments using different scavengers, the authors showed that $^{\bullet}OH$, $^{\bullet}O_2^-$ and h^+ are the active species for this process, with the major contribution of the photogenerated holes. The synergistic effect of combining pyrene and porphyrin is ascribed to an efficient and sequential electron and energy transfer between pyrene, porphyrin and the inorganic SBU, resulting in an improved charge separation. In addition, nMLM maintained the photocatalytic performance after three recycling tests on RhB degradation; however the material was not characterized after the recycling tests.

Bisphenol compounds

Bisphenol compounds (BPs) represent another group of extensively studied targets for photocatalytic degradation using PMOFs (Table 5). The most common bisphenols found in polluted waters are bisphenol A (BPA), an organic molecule often used in plastics and resins fabrication,[135] and bisphenol F (BPF), an analogue molecule used as a substitute for BPA.[136] Extensive monitoring of BPA in various environmental media has been conducted over the last years. In 2009, a statistical analysis considering 89 investigations concluded that the median environmental BPA concentrations for fresh surface water for North America and Europe were 0.081 and 0.01 μg L^{-1}, respectively.[137] Although these values remain below the available regulatory criteria (1.5 and 0.15 μg L^{-1}, respectively), the elimination of these types of pollutant has to be addressed since BPs are endocrine disruptors and present highly toxic effects in living organisms.[138]

A literature survey and normalization of the results (Table 5) show that Zr-based PMOFs are the most effective in BPA photocatalytic degradation. As addressed in the introduction, several topologies can be obtained when combining TCPP ligand with a Zr_6 node, in closely related conditions including PCN-223, PCN-224, PCN-225, and MOF-525, corresponding to the **shp**, **she**, **sqc**, and **ftw** topologies, respectively. In these syntheses, the amount of used modulator (mono-carboxylic acid) is a critical parameter to drive specific MOF phase formation. The influence of the topology on the photocatalytic degradation performance of BPA was investigated by Li and coworkers.[139] The morphology of synthesized PCN-223, PCN-224, PCN-225, and MOF-525 solids was characterized by SEM as cubic (500 nm), cubic (300 nm), rod-shaped (7 × 2 μm) and cubic (5 μm) crystallites, respectively. Through XPS and N_2 sorption analysis, the authors found that MOF-525 has a much higher C=O content (around 74.36%) and a larger (S_{BET} of 2167 $m^2\ g^{-1}$) compared with the other three phases. From the series, PCN-225 and MOF-525 were efficient in the degradation of BPA at variable pH conditions (pH = 3–9) and high salinity (in the presence of NaCl, Na_2SO_4, $NaNO_3$ or $NaHCO_3$). The results showed high rates of BPA elimination (98 and 100% for PCN-225 and MOF-525, respectively), probably due to the important BPA adsorption (76 and 78%, respectively) associated with the very high MOF surface areas (2167 and 1080 $m^2\ g^{-1}$).[139] In the case of MOF-525, it was proposed that a high number of structural defects (lack of TCPP linkers) results in the decrease of the energy level of Zr atoms, facilitating the charge transfer for the photocatalysis process. The BPA photodegradation mechanism was investigated (Fig. 20), and the use

Table 5 PMOFs for the photocatalytic degradation of bisphenol compounds

	PMOFs	Metal	S_{BET} (m^2 g^{-1})	Photosource	BP type; concentration (mg L^{-1}); volume (mL)	Catalyst amount (mg)	Degradation; Initial adsorption (%)	Normalized activity[a] (μg removed pollutant mg^{-1} catalyst h^{-1})	Adsorption time; irradiation time (h)	Number of cycles	Ref., year
3D-PMOFs	PCN-223	Zr	450	500 W Xe lamp λ > 420 nm	BPA; 15; 100	10	69; 2	103	1; 0.5	NM	139, 2022
	PCN-224		140				38; 25	57		NM	
	PCN-225		1080				98; 76	147		NM	
	MOF-525		2167				100; 78	150		6	
	PCN-223		143	500 W Xe lamp λ > 420 nm	BPF; 15; 100	40	98; NM	20	2; 1	8	142, 2022
Composites	Co-TCPP	Co	153	300 W Xe lamp λ > 420 nm	BPA; 50; 80	20	96; 15	96	2; 1	4	141, 2021
	MOF@B-TiO_2-X							160 (Co-TCPP)			

BPA: Bisphenol A; BPF: Bisphenol F. NM: Not mentioned. [a] Normalized activity: normalized data calculated by μg removed pollutant per mg catalyst per h.

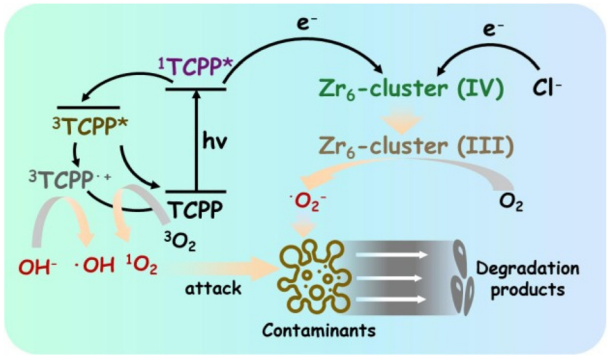

Fig. 20 Scheme of the degradation of contaminants using Zr-based PMOFs. Reproduced from ref. 139 with permission from *Elsevier*, copyright 2022.

of *p*-BQ scavenger evidenced the predominant role of $^{\bullet}O_2^-$ active species. On the other hand, the attenuation of the BPA degradation after the addition of L-histidine (LH) (only scavenging $^1O_2$) indicated the essential role of the singlet oxygen when the addition of $Na_2C_2O_4$ demonstrated the contribution of photogenerated holes. Furthermore, the BPA degradation was poorly influenced in presence of the $K_2C_2O_7$ scavenger, associated with the contribution of e^- and $HO^{\bullet}$.[140] Recyclability experiments of MOF-525 reached 80% pollutant removal efficiency after 6 consecutive cycles, although the crystallinity of the sample was affected as indicated by peak broadening. Additionally, XPS studies revealed a partial oxidation of the MOF upon recycling. Interestingly, the extent of material degradation was found to be lower in NaCl-containing water, closer to real complex conditions in wastewater, and leading to a better recovery of the materials' activity.

A 2D PMOF composite was also used for BPA photocatalytic degradation. Here, the 2D Co-TCPP MOF consisting of a layered structure formed by the coordination of TCPP to four Co paddlewheel metal nodes ($Co_2(COO)_4$), was decorated with 2D black TiO_2 (B-TiO_{2-x}) nanosheets.[141] In contrast to the positive results observed for dye elimination, the combination of the MOF with the semiconducting nanoparticles in Co-TCPP MOF@B-TiO_{2-x} led to a lower BPA removal (estimated at only 96 μg mg^{-1} h^{-1}) when compared with 3D single MOF materials (Table 5). As mentioned previously, a comparison is challenging since our calculations assume a linear relationship between the amount of removed pollutant and the light-exposure time, which is not always true. In order to consider comparable exposure times, normalized data were also calculated for the composite after 1 h irradiation, reaching a value within the same range as the pristine Co-TCPP material (160 μg mg^{-1} h^{-1}), which is a good catalytical performance considering the lower lamp intensity (300 *vs.* 500 W). The effective photocatalytic performance of the composite is *a priori* due to the presence of oxygen vacancies on B-TiO_{2-x}, expanding the visible light absorption to the infrared region due to the presence of Ti^{3+} and oxygen vacancies. The authors corroborated this fact by observing an increase in the degra-

dation performances when using a larger amount of catalyst, up to a limit in which the catalyst could lead into visible light exposure blockage, resulting in lower contaminant removal. Degradation tests performed with variable concentrations of BPA showed that the degradability increased from 60 to 99% in a 2 h reaction time, with an initial BPA concentration decreasing from 90 to 10 mg L^{-1}. This demonstrates the influence of the pollutant concentration for both adsorption and photocatalytic performances. The composite showed stable photocatalytic activity over four cycles, with preserved crystallinity. However, the cyclability study was conducted in distilled water, and the material's performance may differ in real wastewater conditions where diverse organic contaminants, ionic species, and/or organic matter are present.

Pharmaceuticals

Pharmaceutical products include all compounds used to prevent, treat or alleviate symptoms caused by a disease or ailment (anti-inflammatory drugs, antiepileptics, statins, antiepileptics, hormones, beta-blockers, antibiotics, antidepressants, contrast agents, veterinary drugs, *etc.*).[143,144] Although these substances are essential to human and animal health, low concentrations of these compounds as well as their metabolites or degradation products can produce physiological alterations in organisms living in polluted waters and can also reach humans.[145] Furthermore, the poor removal of pharmaceuticals in wastewater treatment plants makes them priority substances in decontamination processes. In this regard, the EU commission has recently published an amendment on the Water Framework Directive incorporating pharmaceuticals (among other substances) as a priority group in water management and in the determination of environmental quality standards.[146] Several studies quantified these compounds in the environment, obtaining alarming high concentrations, especially in water bodies in which wastewater is disposed. Regarding PMOFs, they became a hot topic for the degradation of this kind of contaminant as evidenced by the number of reports summarized in Table 6.

In a recent work, an iron-based PMOF (Fe-TCPP), consisting of TCPP ligands and Fe_3 clusters ($Fe_3O(COO)_6$), was synthesized in a nanorod shape using a surfactant-assisted solvothermal procedure. Considering the normalized data presented in Table 6, Fe-TCPP presents the best removal capacities, surpassing the rest of the reviewed reports. Notably, it achieved 100% of ciprofloxacin (CIP) elimination in only 40 minutes under a 300 W Xe lamp irradiation, corresponding to a normalized value of 631 μg mg^{-1} h^{-1}.[147] Although details on the contribution of the adsorption step are lacking, it should be noted that the potential incomplete solvent elimination during the activation process (60 °C under vacuum overnight) results in a low accessible porosity (34 m^2 g^{-1}). Consequently, the primary photocatalytic activity of Fe-TCPP in CIP elimination could predominantly be located on the external surface of the particles (2 μm × 100 nm). The reported degradation mechanism is based here on the photo-Fenton reaction in the presence of H_2O_2. The addition of *tert*-butyl alcohol as a scavenger led to a decrease of the degradation rate, highlighting the main contribution of $HO^{\bullet}$ to CIP degradation.[148] The ligand-to-cluster charge transfer favoured the reduction of Fe^{3+} to Fe^{2+}, which in turn generated more $HO^{\bullet}$ by reducing H_2O_2 and enhanced CIP removal rates. The pseudo-first-order reaction kinetic fitting revealed a significant self-enhancement of the rate constant (k) for CIP degradation after 20 minutes, which is attributed to the incremental concentration of accumulated $HO^{\bullet}$ within 40 min. Comparative analysis with other Fe-MOFs tested in photo-Fenton reactions for CIP degradation, such as MIL-100(Fe), demonstrated that Fe-TCPP exhibited kinetic constants 3 and 29 times higher for the first half and second half of the process, respectively, than those achieved by the MIL-100(Fe).[147] The potential iron release was monitored for a cycle, obtaining a total leaching value of 0.1 mg L^{-1}, below the fixed environmental concentration standards (0.3 mg L^{-1}).[149] The authors demonstrated that 85% of the removal efficacy was maintained after 5 cycles, suggesting a partial catalyst poisoning. Furthermore, PXRD and SEM results revealed that the morphology and structure of the material did not significantly change throughout the cycles, although a decrease in crystallinity was observed.

In a different study, a series of PCN-224 with different particles sizes (150, 300, 500, and 6000 nm) was prepared by adjusting the synthesis parameter (*i.e.*, amount of modulator, synthesis temperature, time). The materials were then examined for CIP removal from water. The 300 nm particle size PCN-224 reached the best performance with an 84% removal within 3 h, but corresponding to a relatively low normalized value of 33 μg mg^{-1} h^{-1}.[150] When compared with the previous Fe-TCPP, the degradation rate of PCN-224 is notably lower, despite its much higher S_{BET} (1616 m^2 g^{-1} *vs.* 34 m^2 g^{-1}), and the use of a more intense light source (500 *vs.* 300 W Xe lamp). However, the adsorbed CIP content prior to light irradiation was not specified. Furthermore, PCN-224 was able to degrade tetracycline (TCL), a well-studied molecule in the context of PMOFs (see Table 6), reaching 92% removal and corresponding to 36 μg mg^{-1} h^{-1}. The photodegradation properties of both CIP and TCL by PCN-224 remained stable over 5 consecutive cycles. Considering the potential influence of a mixture of contaminants on the elimination capacity of MOFs, such research should be encouraged. It is interesting to highlight here the TCL degradation performance of the (2D) Cu-TCPP (S_{BET} = 343 m^2 g^{-1}) which exhibited a twice higher normalized value (62 μg mg^{-1} h^{-1} after 6 h), in comparison with PCN-224.[123]

TCL degradation capacity significantly increases when PMOF-based composites are used as photocatalysts. As already discussed for the case of dye degradation, the presence of semiconducting NPs on PMOF structures generally enhances the catalytical activity of the materials by promoting an efficient interaction between the electronic bands of both materials.[127,128] A relevant example is the $ZnIn_2S_4$/MOF-525 composite (S_{BET} = 225 m^2 g^{-1}), which achieved a 94% TCL removal within 1 h under visible light irradiation (300 W Xe lamp).[151] Prior to irradiation, an adsorption/desorption equili-

Table 6 PMOFs in pharmaceutical photocatalytic degradation

	PMOFs	Metal	S_{BET} (m^2 g^{-1})	Photosource	Pollutant; concentration (mg L^{-1}); volume (mL)	Catalyst amount (mg)	Degradation; Initial adsorption (%)	Normalized activity[a] (μg removed pollutant mg^{-1} catalyst h^{-1})	Adsorption time; irradiation time (h)	Cycle	Ref.; year
2D-PMOF	Cu-TCPP	Cu	343	300 W Xe lamp $\lambda \geq 420$ nm	OTC; 40; 100 TCL; 40; 100 NFX; 20; 100	5	86 47 44	115 62 29	6; 2	NM	123, 2020
3D-PMOF	PCN-134	Zr	756	500 W Xe lamp $\lambda \geq 420$ nm	DF; 30; 50	5	>99	59	5; 3	3	153, 2016
	PCN-134(Fe)	Zr	1450	Xe lamp Simulated solar light	AT, CA, DF, IBU & SSM; 0.1; 30; 30 NPX; 40; 25	5	81; 59 86; 41 98; 86 97; 91 81; 49 NPX; >95; 0	0.162 0.172 0.196 0.194 0.162 82	3; 1 NPX; 2.3; 0.3	NM	154, 2023
	Hf-TCPP-FA	Hf	1740	350 W Xe lamp $\lambda \geq 400$ nm	NFX; 10; 100	10	94	62	1; 0.5	6	155, 2023
	PCN-224	Zr	1616	500 W Xe lamp $\lambda \geq 420$ nm	TCL; 30; 4 CIP; 30; 4	1	92 84	36 33	3; 1	5	150, 2021
	Fe-TCPP	Fe	34	300 W Xe lamp $\lambda \geq 420$ nm	CIP; 25; 50	3	100	631	0.6; 0.6	5	147, 2022
Composites	$ZnIn_2S_4$/MOF-525	Zr	225	300 W Xe lamp $\lambda \geq 420$ nm	TCL; 20; 100	15	94; 40	125	1; 0.6	5	151, 2023
	2N-CDs@PCN-222@PNIPAM	Zr	288	300 W Xe lamp $\lambda \geq 420$ nm	TCL; 20; 100	50	91; 75	110	0.3; 0.5	5	130, 2021
	Ag@MOFs	Zr	2250	500 W Xe lamp $\lambda \geq 420$ nm	TCL; 10; 50	50	81	20	3.3; 1	4	134, 2023
	TCPP@PCN-777-30	Zr	1300	Xe lamp 21.06 mW cm^{-2}	RND; 6.3; 50	5	>99; 20	62	1; 1	4	156, 2022

AT: antipyrine; CA: clofibric acid; CIP: ciprofloxacin; DF: diclofenac; IBU: ibuprofen; NFX: norfloxacin; NPX: naproxen; OTC: oxytocin; RND: ranitidine; SSM: sulfadimethoxypyrimidine; TCL: tetracycline. NM: Not mentioned. [a] Normalized activity: normalized data calculated by μg removed pollutant per mg catalyst per h.

brium was reached after 40 minutes with 40% of TCL adsorbed. The total elimination reached 94%, corresponding to 125 μg mg^{-1} h^{-1}. The proposed mechanism involves the major role of $^{\bullet}O_2^-$ and holes in the photocatalytic process. Both active species participate in the oxidation of TCL, eventually breaking it down to H_2O, CO_2 and other small molecular substances.[151]

Similarly, a composite material 2N-CDs@PCN-222@PNIPAM (S_{BET} = 288 m^2 g^{-1}) achieved 91% of TCL elimination under the same irradiation conditions. This corresponds to a normalized value of 110 μg mg^{-1} h^{-1} close to the previous composite. The initial TCL adsorption step in this case reached 75%.[130]

Mixed linker Zr-based MOFs have also been considered for the photodegradation of pharmaceuticals. PCN-134 is based on a layer–pillar structure, where 2D layers are formed by the coordination of Zr_6 clusters with benzene-1,3,5-tribenzoate (BTB) and then connected by TCPP pillars. The occupancy of the pillar porphyrins can be varied to a certain degree allowing the isolation of defective materials with tuneable sorption properties.[152] In 2019, PCN-134 was studied for the elimination of diclofenac (DF) by Gao *et al.*[153] Note that the synthesized material presents lower crystallinity and S_{BET} than in the initial report (756 *vs.* 1946 m^2 g^{-1}). The effect of the amount of TCPP defects on the sorption capacities was investigated, and the highest DF uptake (0.7 mmol g^{-1}) was observed for a TCPP molar ratio of 30% (33.3% for the defect-free structure). The effect of NaCl addition to the DF aqueous solutions was found to be detrimental through inhibiting the electrostatic interactions between the DF molecules and the MOF. The photocatalytic activity towards DF degradation under a 500 W Xe lamp reached a removal rate >99% in 5 h and the recyclability tests showed a 95% removal at the third cycle. However, the material was not characterized after photocatalysis. Interestingly, the scavenging experiments evidenced that the mixed linker MOF was highly efficient for singlet oxygen production in comparison with a single TCPP-based counterpart (PCN-224).

More recently, free-base, Fe and Cu metalloporphyrin versions of PCN-134 (S_{BET} = 1450, 443 and 933 m^2 g^{-1}, respectively) were considered for the simultaneous removal of 5 different pollutants (antipyrine – AT, clofibric acid – CA, diclofenac – DF, ibuprofen – IBU and sulfadimethoxypyrimidine – SSM), simulating the conditions (0.1 ppm) found in wastewater (Fig. 21).[154] However, distilled water was used to prepare the contaminant solutions. The Fe and Cu modified versions of PCN-134 showed improved performances in terms of adsorption rates and degradation efficiency. For instance, in the case of PCN-134(Fe), after 3 h under simulated sunlight irradiation, respective removals of 81, 86, 98, 97 and 81% for AT, CA, DF, IBU and SSM were achieved. Note the major contribution of the initial adsorption step to the removal efficiency as it accounted for 59, 41, 86, 91 and 49% removal, respectively. Although the normalized values are extremely low in comparison with other reports (Table 6), all the targeted pollutants were removed at high percentages from the media, reaching

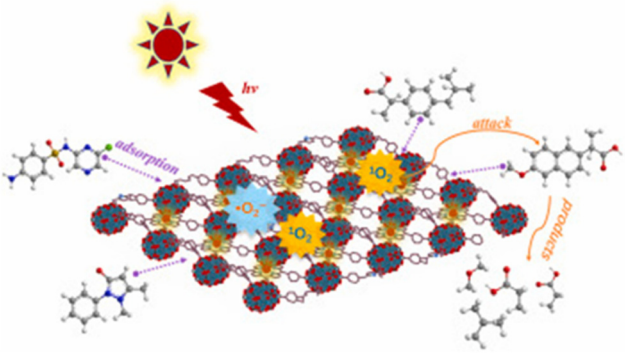

Fig. 21 Simultaneous adsorption and photodegradation of different pharmaceutical molecules by PCN-134. Reproduced from ref. 154 with permission from *Elsevier*, copyright 2023.

almost complete elimination for DF and IBU. High-performance liquid chromatography coupled to mass spectrometry (HPLC-MS) was used to study the degradation process, identifying the intermediate species. Also, quenching experiments were applied to get insight into the related mechanism, proposing $^{\bullet}O_2^-$ and $^1O_2$ as the major reactive species for the photocatalytic degradation. In addition, the material preserved its crystallinity after photocatalysis as evidenced by PXRD.

In short, all these results demonstrated the potential of the PMOF-based composites for the elimination of pharmaceuticals from water.

Heavy metals

Beyond the EOCs category, PMOFs and PMOF-containing composites have been investigated in water remediation for the removal of heavy metals through photocatalytic reduction. Particularly, PMOFs have been primarily studied for the elimination of the Cr^{6+} ion, commonly used in industrial processes and known for its high water solubility, toxicity and carcinogenic nature.[157,158] Its reduced form, Cr^{3+}, is less harmful and can be easily precipitated as $Cr(OH)_3$ to be removed from water under neutral or alkaline conditions.[159]

In this way, PCN-222(M) (M = H_2, Zn^{2+}, Cu^{2+}, Ni^{2+}, Co^{2+}, Fe^{3+}, and Mn^{3+}) was used as a catalyst for the Cr^{6+} reduction reaction.[160] After 1 h-equilibrium, a $K_2Cr_2O_7$ aqueous solution (10–20 ppm) mixed with methanol was irradiated using three 18 W white LED lamps (>400 nm). Within 25 minutes, a notable 100 and 76% of Cr^{6+} reduction was achieved for PCN-222(H_2) and PCN-222(Zn), respectively. The authors argued that the presence of methanol in the reaction media enhanced the scavenging of holes, facilitating the photogenerated electron transfer to the Zr–O catalytic site which reduces Cr^{6+} to Cr^{3+}. Moreover, PCN-222(H_2) preserved 95% of its catalytic activity after ten consecutive cycles. Structural analysis through PXRD, FTIR and UV-Vis spectroscopy confirmed the preservation of the framework structure.

In a different study, PCN-222(M) (M = H_2, Zn^{2+}, Fe^{3+}, Co^{2+}) was used in a sonophotocatalysis setup (Fig. 22).[161] Sonophotocatalysis was proved effective in preventing the

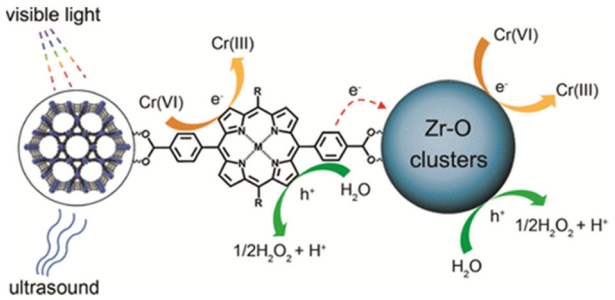

Fig. 22 Photocatalytic reduction scheme of Cr^{6+} to Cr^{3+} using PCN-222 materials as catalysts throughout sonophotocatalytic processes. Reproduced from ref. 161 with permission from *American Chemical Society*, copyright 2021.

agglomeration of the heterogeneous photocatalysts and accelerating the mass transfer of reactants, as well as removing surface impurities through the formation of gas bubbles. The experimental procedure involved an initial 1 h adsorption step, followed by visible light irradiation (300 W Xe lamp) and ultrasound treatment (20 kHz, vibration intensity of 30–120 W). While PCN-222(Zn) and PCN-222(H_2) allowed the removal of 94.2 and 93.8% Cr^{6+}, respectively, PCN-222(Fe) exhibited the lowest Cr^{6+} conversion of just 59.7%. These results agree with the low PC response observed for PCN-222(Fe), indicating that the incorporation of paramagnetic Fe^{3+} ions in porphyrin ligands reduces the charge photogeneration in the MOF. The proposed reduction mechanism involved a light-triggered charge transfer from the porphyrin excited state to the Zr–O catalytic centre that is capable of reducing Cr^{6+} to Cr^{3+}. The simultaneous use of light and ultrasound accelerated the mass transfer, promoting the interaction between the Cr^{6+} and the catalytic active sites of the PCN-222 (Fig. 22). The recyclability of the catalyst was demonstrated through 3 consecutive cycles maintaining efficient Cr^{6+} elimination rates.

Based on this, it can be deduced that among the PCN-222 series, PCN-222(H_2) and PCN-222(Zn) emerge as highly effective catalysts for Cr^{6+} reduction, reaching conversions rates exceeding 94% in notably short reaction times (40 and 30 min, respectively). A remarkable efficiency was maintained in the first example,[160] whereas a gradual loss of activity (from 94 to 90% of elimination after 3 cycles) in the latter case could be due to the harsher conditions related to the ultrasound treatment.

Bacteria

Bacteria comprise an important source of water pollution, being the origin of severe health issues and waterborne diseases.[162] Different techniques (*e.g.* chlorination, ozonation, chlorine dioxide or coagulation) are normally applied to purify water. However, we should consider that these technologies' limitations rely on the toxic disinfection byproducts that are often generated.[163] In that sense, the use of catalysts for the acceleration of pathogen inactivation has become an interesting green alternative to conventional methods.[164–166] Regarding catalytic disinfection, few recent works describe the bactericidal effect of PMOFs under irradiation. This is the case of the 2D layered material (2D)-ZnTCPP, previously referred to in this review for its bisphenol removal capacities, which is able to eliminate >99.99% of an *Escherichia coli* colony (10^7 CFU mL^{-1}; CFU: colony forming unit) when using a concentration of 128 μg mL^{-1} of the catalyst under Xe lamp irradiation (100 mW cm^{-2}) for 30 min.[122] Another reported work illustrates the capacity of PMOF GXNU-1 to reduce by 95% the initial concentration of a *Staphylococcus aureus* colony (~2 × 10^8 CFU mL^{-1}) under light irradiation (60 mW cm^{-2}) when in the presence of 5 mg mL^{-1} of the catalyst for 30 min.[167] A PMOF-containing heterojunction material, composed of Prussian Blue and PCN-224, also demonstrated very effective sterilizing rates for the elimination of *Staphylococcus aureus* and wound healing activity under visible light irradiation.[168] In all these cases, the effective antibacterial effect is a consequence of the large amount of ROS generated upon the PMOFs' irradiation, and these are considered very active species for pathogen and bacterial inactivation.

To summarize, this section highlights that PMOFs have emerged as promising class of photocatalysts for water contaminant removal. In particular, the incorporation of semiconducting NPs in PMOF-composites has proved to be a relevant strategy for enhancing pollutant (such as dyes and pharmaceuticals) photodegradation by promoting charge separation. Incorporating metalated porphyrins as MOF ligands has sometimes been shown to facilitate electron transfer from the metalloporphyrin excited state to the catalytic centre of the MOF (metal clusters). However, the complexity of the photophysical processes involved in the photocatalytic reaction path raises challenges in finely designing and tuning materials for improved activity without compromising the chemical stability. Moreover, comparing TOFs in the reported studies is difficult due to varying conditions and a lack of experimental details (*e.g.* composition, accessibility of the active sites). Nevertheless, PCN-222(Hf) has emerged as one of the best-performing PMOFs for contaminant removal, exhibiting an excellent performance of 2.8 and 2.1 mmol $mmol^{-1}$ h^{-1} for BV14 and RhB removal, respectively, as well as good values for CV and AB210 dyes (1.3 and 0.7 mmol $mmol^{-1}$ h^{-1} respectively). Beyond EOC removal, related issues of water decontamination have been successfully tackled, such as the photocatalytic Cr^{6+} reduction to its less harmful trivalent form. Other related examples include water sterilization, in which PMOFs[122] or their composites[168] are exploited to generate ROS capable of killing bacteria. Freshwater was also harvested by solar evaporation using the photothermal effect of a PMOF;[169] however this last topic remains for now far less studied. Overall, PMOFs offer a wide range of possibilities for effective water decontamination.

D. Conclusions and outlook

Porphyrins belong to the unique class of tetrapyrrolic compounds that have found application for the construction of artificial photosynthetic systems. Advances in designing and

synthesising coordination chemistry networks have paved the way for water-stable, porous and functional architectures. In this context, PMOFs have exhibited remarkable potential over the past decade as active and stable photocatalysts for the solar-driven production of fuels and the degradation of pollutants in water.

In the field of solar fuel generation, PMOFs have been extensively employed as photocatalysts for the HER in the presence of SEDs. The achieved results indicate that PMOFs exhibit outstanding activities under solar light irradiation when compared with other MOFs. This is mainly attributed to their capability to absorb a broad range of visible light, as well as the ability to chelate relevant metal ions inside the porphyrinic core as single metal atom sites.

Since their initial application in 2012, PMOFs as HER photocatalysts have witnessed a substantial increase in examples, with most of the water-stable photocatalysts being built with Al^{3+}, Zr^{4+} or Ti^{4+} as well as In^{3+} or Ru^{2+} metals together with porphyrin-based organic ligands like TCPP. A common strategy to enhance their photocatalytic activity involves the deposition of metallic NPs as specific HER co-catalysts that improve the photoinduced charge separation efficiency. Importantly, some examples have shown that metalation of the porphyrin core with single atoms like Pt results in more active photocatalysts compared with the use of metallic NPs. Recent reports have explored PMOF composites with materials like CN, resulting in more efficient heterojunction photocatalytic systems compared with the individual constituents. Remarkably, since 2021, a few studies have shown the possibility of using PMOFs as photocatalysts for solar-driven OWS into H_2 and O_2 although the obtained efficiencies remain, for now, far from industrial applications.

Despite these considerations, MOFs and specifically PMOFs stand out as the most versatile porous materials available so far. Anticipated developments in the coming years include tailoring PMOFs and PMOF-based composites energy band diagrams through synthesis and post-synthesis methods along with the combination of *in situ* characterization, to meet the thermodynamic requirements of the OWS under sunlight irradiation. For example, the functionalization of the porphyrinic ligands can be used to modify the HOCO level and enhance the efficiency of H_2O oxidation to O_2. Similarly, preparing mixed-metal nodes can be employed as a strategy to adjust the LUCO position, affecting the proton reduction reaction performance. Employing PMOFs with two selective co-catalysts for the HER and OER represents a promising approach to enhance overall process efficiency. Another encouraging pathway involved developing PMOF heterojunctions with suitable energy band level diagrams to improve photoinduced charge separation and OWS efficiency. Overall, dynamic research is expected to drive the field of solar fuel production using PMOFs as photocatalysts, particularly in the context of H_2O splitting into H_2 and O_2 using solar light irradiation.

Regarding water decontamination, current research predominantly focuses on fundamental aspects including adsorption, catalytic performances and underlying mechanisms. In addition, a growing number of studies explore close-to-real pollution conditions, aiming to eliminate a mixture of contaminants while assessing the reusability of PMOFs to demonstrate their potential in this area.

However, analogous to solar fuel production applications, the promising research is still in its early stages and far from practical applications. In this sense, it is imperative to highlight the lack of key information in some reports, such as the nature of the water source, the catalyst particle size, cocatalyst content, identification and toxicological evaluation of degradation products and quantitative assessment of potential metal/ligand leaching from PMOFs during degradation. These details are crucial for evaluating the practical utility of PMOFs. Additionally, realistic aspects, such as the use of wastewater containing a complex mixture of organic and inorganic contaminants, continuous flow operation conditions and long-term recyclability and regeneration tests (>100 cycles), need further investigation for real-scale applications. The significant challenges associated with implementing PMOFs in actual industrial processes encompass operational optimization, device development and cost considerations (*e.g.* precursors, safe and efficient scale-up, shaping, devices). In this sense, utilizing sunlight as an energy source can significantly reduce operational costs.

These challenges are inherent to the novelty of the research field. In this context, photocatalytic properties of porphyrins and their ability to activate molecular oxygen have already been successfully applied in pilot units for either a well-established hydrocarbon oxidation process[170] or an advanced fine chemical synthesis of artemisinin (malaria treatment drug).[171] Moreover, it is crucial to strike a balance between the cost considerations and societal evolution leading to new health and environment regulations. Regarding efficiency, MOFs demonstrate significant technological advancements for eliminating emerging contaminants compared with existing processes. From this perspective, PMOF-based materials hold substantial potential for providing innovative solutions to address emerging pollutants in real contaminated waters.

Finally, an emerging trend draws closer the two applications by adopting the dual-functional photocatalysis approach, wherein the HER for solar fuel production is synergistically combined with the oxidative photodegradation of pollutants.[172] This innovative strategy offers the potential to substitute SEDs by toxic pollutants. While this strategy is currently limited regarding PMOFs, dynamic scientific progress is anticipated in this area.

List of acronyms

AB210	Acid black 210
AQY	Apparent quantum yield
AT	Antipyrine
BDC	1,4-Benzenedicarboxylate
BET	Brunauer–Emmett–Teller
BPA	Bisphenol A
BPF	Bisphenol F

BPs	Bisphenol compounds
BTB	Benzene-1,3,5-tribenzoate
BV14	Basic violet 14
CA	Clofibric acid
CDs	Carbon dots
CIP	Ciprofloxacin
CN	Carbon nitride
CR	Congo red
COF	Covalent-organic framework
CV	Crystal violet
DF	Diclofenac
DFT	Density functional theory
DMF	*N*,*N*-Dimethylformamide
DPBF	1,3-Diphenylbenzofuran
EDX	Energy dispersive X-ray
EIS	Electrochemical impedance spectroscopy
EOCs	Emerging organic contaminants
EPR	Electron paramagnetic resonance
EryB	Erythrosin B
EU	European Union
FTIR	Fourier transform infrared spectroscopy
GC-MS	Gas chromatography-mass spectrometry
HER	Hydrogen evolution reaction
HOCO	Highest occupied crystal orbital
HPLC-MS	High-performance liquid chromatography coupled to mass spectrometry
HSAB	Hard and soft acids and bases
IBU	Ibuprofen
ICP-MS	Inductively coupled plasma mass spectrometry
ICP-OES	Inductively coupled plasma optical emission spectroscopy
IPA	Isopropanol
LH	L-Histidine
LMCT	Ligand-to-metal charge transfer
LUCO	Lowest unoccupied crystal orbital
MB	Methylene blue
MNSs	MOF nanosheets
MO	Methyl orange
MOFs	Metal-organic frameworks
NFX	Norfloxacin
NHE	Normal hydrogen electrode
nMLM	Nanosized mixed-ligand MOF
NMR	Nuclear magnetic resonance
NPs	Nanoparticles
NPX	Naproxen
OER	Oxygen evolution reaction
OTC	Oxytocin
OWS	Overall water splitting
p-BQ	*para*-Benzoquinone
PC	Photocurrent
PL	Photoluminescence
PMOFs	Porphyrin-based metal–organic frameworks
PNIPAM	Poly(*N*-isopropylacrylamide)
PVDF	Polyvinylidene fluoride
PXRD	Powder X-ray diffraction
RhB	Rhodamine B
RND	Ranitidine
ROS	Reactive oxygen species
RoseB	Rose Bengal
SBU	Secondary building unit
SED	Sacrificial electron donors
SEM	Scanning electron microscopy
SSM	Sulfadimethoxypyrimidine
STEM	Scanning transmission electron microscopy
STH	Solar-to-hydrogen
TA	Tannic acid
TAS	Transient absorption spectroscopy
TBP	5,10,15,20-tetra(p-benzoic acid)porphyrin
TCL	Tetracycline
TCPP	Tetrakis(4-carboxyphenyl)porphyrin
TEM	Transmission electron microscopy
TEOA	Triethanolamine
TGA	Thermogravimetric analysis
TNTs	Titanate nanotubes
TOF	Turnover frequency
TON	Turnover number
TRPL	Time-resolved photoluminescence
UV-Vis	Ultraviolet–visible spectroscopy
WOR	Water oxidation reaction
XANES	X-ray absorption near edge structure
XPS	X-ray photoelectron spectroscopy
XRD	X-ray diffraction

Conflicts of interest

There are no conflicts to declare.

Acknowledgements

A. F. thanks the support of LABEX iMust ANR-10-LABX-0064, of the University Lyon 1 and CNRS. This work was supported by the Arqus European University Alliance, co-funded by the European Commission, and by a grant from the French government managed by the ANR under the Investissements d'avenir programme, ANR-19-GURE-00013 and of the ARQUS European University Alliance. F. L. thanks the China Scholarship Council. H. G. thanks Ayuda RYC2022-037287-I financiada por MCIN/AEI/10.13039/501100011033 y por El FSE invierte en tu future. A. D. is beneficiary of a grant María Zambrano in Universitat Politècnica de València within the framework of the grants for retraining in the Spanish university system (Spanish Ministry of Universities, financed by the European Union, NextGeneration EU). P. H. and S. R. thank the support of the projects MOFseidon PID2019-104228RB-I00, ESENCE RTC2019-007254-5, NAPOLION PID2022-139956OB-I00 and MOFCycle CNS2022-135779 funded by MCIN/AEI/10.13039/501100011033 and by ERDF A way of making Europe. S. R. is grateful for the support of B-FQM-394, and ProyExcel_00105 funded from Junta de Andalucía, and the grant (RYC2021-032522-I) funded by MCIN/AEI/10.13039/

501100011033 and for El FSE invierte en tu future. S. N. thanks the support of grant PID2021-123856OBI00 funded by MICIU/AEI/10.13039/501100011033 and by ERDF A way of making Europe. The METHASOL project receives funding from the European Union Horizon 2020 research and innovation programme under Grant Agreement N°101022649.

References

1 A. R. Battersby, Tetrapyrroles: the pigments of life, *Nat. Prod. Rep.*, 2000, **17**, 507–526.
2 S. Lesage, H. Xu and L. Durham, The occurrence and roles of porphyrins in the environment: possible implications for bioremediation, *Hydrol. Sci. J.*, 1993, **38**, 343–354.
3 I. Galván, P. R. Camarero, R. Mateo and J. J. Negro, Porphyrins produce uniquely ephemeral animal colouration: a possible signal of virginity, *Sci. Rep.*, 2016, **6**, 39210.
4 C. Camacho, J. J. Negro, I. Redondo, S. Palacios and P. Sáez-Gómez, Correlates of individual variation in the porphyrin-based fluorescence of red-necked nightjars (Caprimulgus ruficollis), *Sci. Rep.*, 2019, **9**, 19115.
5 B. F. Abrahams, B. F. Hoskins and R. Robson, A new type of infinite 3D polymeric network containing 4-connected, peripherally-linked metalloporphyrin building blocks, *J. Am. Chem. Soc.*, 1991, **113**, 3606–3607.
6 B. F. Abrahams, B. F. Hoskins, D. M. Michail and R. Robson, Assembly of porphyrin building blocks into network structures with large channels, *Nature*, 1994, **369**, 727–729.
7 S. De, T. Devic and A. Fateeva, Porphyrin and phthalocyanine-based metal organic frameworks beyond metal-carboxylates, *Dalton Trans.*, 2021, **50**, 1166–1188.
8 X. Zhang, M. C. Wasson, M. Shayan, E. K. Berdichevsky, J. Ricardo-Noordberg, Z. Singh, E. K. Papazyan, A. J. Castro, P. Marino, Z. Ajoyan, Z. Chen, T. Islamoglu, A. J. Howarth, Y. Liu, M. B. Majewski, M. J. Katz, J. E. Mondloch and O. K. Farha, A historical perspective on porphyrin-based metal–organic frameworks and their applications, *Coord. Chem. Rev.*, 2021, **429**, 213615.
9 S. S. Rajasree, X. Li and P. Deria, Physical properties of porphyrin-based crystalline metal-organic frameworks, *Commun. Chem.*, 2021, **4**, 47.
10 Y. G. Gorbunova, Y. Y. Enakieva, M. V. Volostnykh, A. A. Sinelshchikova, I. A. Abdulaeva, K. P. Birin and A. Y. Tsivadze, Porous porphyrin-based metal-organic frameworks: synthesis, structure, sorption properties and application prospects, *Russ. Chem. Rev.*, 2022, **91**, RCR5038.
11 B. Liu, K. Vikrant, K.-H. Kim, V. Kumar and S. K. Kailasa, Critical role of water stability in metal–organic frameworks and advanced modification strategies for the extension of their applicability, *Environ. Sci. Nano*, 2020, **7**, 1319–1347.
12 L. Feng, K.-Y. Wang, G. S. Day, M. R. Ryder and H.-C. Zhou, Destruction of Metal–Organic Frameworks: Positive and Negative Aspects of Stability and Lability, *Chem. Rev.*, 2020, **120**, 13087–13133.
13 A. Fateeva, P. A. Chater, C. P. Ireland, A. A. Tahir, Y. Z. Khimyak, P. V. Wiper, J. R. Darwent and M. J. Rosseinsky, A Water-Stable Porphyrin-Based Metal–Organic Framework Active for Visible-Light Photocatalysis, *Angew. Chem., Int. Ed.*, 2012, **51**, 7440–7444.
14 D. Feng, Z.-Y. Gu, J.-R. Li, H.-L. Jiang, Z. Wei and H.-C. Zhou, Zirconium-Metalloporphyrin PCN-222: Mesoporous Metal–Organic Frameworks with Ultrahigh Stability as Biomimetic Catalysts, *Angew. Chem., Int. Ed.*, 2012, **51**, 10307–10310.
15 D. Feng, W.-C. Chung, Z. Wei, Z.-Y. Gu, H.-L. Jiang, Y.-P. Chen, D. J. Darensbourg and H.-C. Zhou, Construction of Ultrastable Porphyrin Zr Metal–Organic Frameworks through Linker Elimination, *J. Am. Chem. Soc.*, 2013, **135**, 17105–17110.
16 W. Morris, B. Volosskiy, S. Demir, F. Gándara, P. L. McGrier, H. Furukawa, D. Cascio, J. F. Stoddart and O. M. Yaghi, Synthesis, Structure, and Metalation of Two New Highly Porous Zirconium Metal–Organic Frameworks, *Inorg. Chem.*, 2012, **51**, 6443–6445.
17 C. Koschnick, R. Stäglich, T. Scholz, M. W. Terban, A. von Mankowski, G. Savasci, F. Binder, A. Schökel, M. Etter, J. Nuss, R. Siegel, L. S. Germann, C. Ochsenfeld, R. E. Dinnebier, J. Senker and B. V. Lotsch, Understanding disorder and linker deficiency in porphyrinic zirconium-based metal–organic frameworks by resolving the Zr8O6 cluster conundrum in PCN-221, *Nat. Commun.*, 2021, **12**, 3099.
18 G. Mouchaham, B. Abeykoon, M. Giménez-Marqués, S. Navalon, A. Santiago-Portillo, M. Affram, N. Guillou, C. Martineau, H. Garcia, A. Fateeva and T. Devic, Adaptability of the metal(iii,iv) 1,2,3-trioxobenzene rod secondary building unit for the production of chemically stable and catalytically active MOFs, *Chem. Commun.*, 2017, **53**, 7661–7664.
19 M. A. Nasalevich, C. H. Hendon, J. G. Santaclara, K. Svane, B. van der Linden, S. L. Veber, M. V. Fedin, A. J. Houtepen, M. A. van der Veen, F. Kapteijn, A. Walsh and J. Gascon, Electronic origins of photocatalytic activity in d0 metal organic frameworks, *Sci. Rep.*, 2016, **6**, 23676.
20 A. Ortega-Guerrero, M. Fumanal, G. Capano and B. Smit, From Isolated Porphyrin Ligands to Periodic Al-PMOF: A Comparative Study of the Optical Properties Using DFT/TDDFT, *J. Phys. Chem. C*, 2020, **124**, 21751–21760.
21 P. Deria, J. Yu, R. P. Balaraman, J. Mashni and S. N. White, Topology-dependent emissive properties of zirconium-based porphyrin MOFs, *Chem. Commun.*, 2016, **52**, 13031–13034.
22 M. Gouterman, G. H. Wagnière and L. C. Snyder, Spectra of porphyrins: Part II. Four orbital model, *J. Mol. Spectrosc.*, 1963, **11**, 108–127.

23 J. G. Santaclara, F. Kapteijn, J. Gascon and M. A. van der Veen, Understanding metal–organic frameworks for photocatalytic solar fuel production, *CrystEngComm*, 2017, **19**, 4118–4125.
24 S. Navalón, A. Dhakshinamoorthy, M. Álvaro, B. Ferrer and H. García, Metal–Organic Frameworks as Photocatalysts for Solar-Driven Overall Water Splitting, *Chem. Rev.*, 2023, **123**, 445–490.
25 J. H. Kim, D. Hansora, P. Sharma, J.-W. Jang and J. S. Lee, Toward practical solar hydrogen production – an artificial photosynthetic leaf-to-farm challenge, *Chem. Soc. Rev.*, 2019, **48**, 1908–1971.
26 F. Haber, J. Weiss and W. J. Pope, The catalytic decomposition of hydrogen peroxide by iron salts, *Proc. R. Soc. London, Ser. A*, 1997, **147**, 332–351.
27 S. Hamad, N. Hernandez, A. Aziz, A. Ruiz-Salvador, S. Calero and R. Grau-Crespo, Electronic structure of porphyrin-based metal-organic frameworks and their suitability for solar fuel production photocatalysis, *J. Mater. Chem. A*, 2015, **3**, 23458–23465.
28 A. Aziz, A. Ruiz-Salvador, N. Hernandez, S. Calero, S. Hamad and R. Grau-Crespo, Porphyrin-based metal-organic frameworks for solar fuel synthesis photocatalysis: band gap tuning via iron substitutions, *J. Mater. Chem. A*, 2017, **5**, 11894–11904.
29 V. Posligua, D. Pandya, A. Aziz, M. Rivera, R. Crespo-Otero, S. Hamad and R. Grau-Crespo, Engineering the electronic and optical properties of 2D porphyrin-paddlewheel metal-organic frameworks, *JPhys Energy*, 2021, **3**, 034005.
30 A. Ortega-Guerrero, M. Fumanal, G. Capano, I. Tavernelli and B. Smit, Insights into the Electronic Properties and Charge Transfer Mechanism of a Porphyrin Ruthenium-Based Metal-Organic Framework, *Chem. Mater.*, 2020, **32**, 4194–4204.
31 J. Li, R. Güttinger, R. Moré, F. Song, W. Wan and G. R. Patzke, Frontiers of water oxidation: the quest for true catalysts, *Chem. Soc. Rev.*, 2017, **46**, 6124–6147.
32 A. Dhakshinamoorthy, A. M. Asiri and H. Garcia, 2D Metal–Organic Frameworks as Multifunctional Materials in Heterogeneous Catalysis and Electro/Photocatalysis, *Adv. Mater.*, 2019, **31**, 1900617.
33 J. Nicks, K. Sasitharan, R. R. R. Prasad, D. J. Ashworth and J. A. Foster, Metal–Organic Framework Nanosheets: Programmable 2D Materials for Catalysis, Sensing, Electronics, and Separation Applications, *Adv. Funct. Mater.*, 2021, **31**, 2103723.
34 L. S. Xie, G. Skorupskii and M. Dincă, Electrically Conductive Metal–Organic Frameworks, *Chem. Rev.*, 2020, **120**, 8536–8580.
35 M. Wang, R. Dong and X. Feng, Two-dimensional conjugated metal–organic frameworks (2D c-MOFs): chemistry and function for MOFtronics, *Chem. Soc. Rev.*, 2021, **50**, 2764–2793.
36 Y. Xue, G. Zhao, R. Yang, F. Chu, J. Chen, L. Wang and X. Huang, 2D metal–organic framework-based materials for electrocatalytic, photocatalytic and thermocatalytic applications, *Nanoscale*, 2021, **13**, 3911–3936.
37 L. Wang, S. E. Saji, L. Wu, Z. Wang, Z. Chen, Y. Du, X. Yu, H. Zhao and Z. Yin, Emerging Synthesis Strategies of 2D MOFs for Electrical Devices and Integrated Circuits, *Small*, 2022, **18**, 2201642.
38 S. Haussener, Solar fuel processing: Comparative mini-review on research, technology development, and scaling, *Sol. Energy*, 2022, **246**, 294–300.
39 J.-D. Xiao, R. Li and H.-L. Jiang, Metal–Organic Framework-Based Photocatalysis for Solar Fuel Production, *Small Methods*, 2023, **7**, 2201258.
40 Z.-B. Fang, T.-T. Liu, J. Liu, S. Jin, X.-P. Wu, X.-Q. Gong, K. Wang, Q. Yin, T.-F. Liu, R. Cao and H.-C. Zhou, Boosting Interfacial Charge-Transfer Kinetics for Efficient Overall CO2 Photoreduction via Rational Design of Coordination Spheres on Metal–Organic Frameworks, *J. Am. Chem. Soc.*, 2020, **142**, 12515–12523.
41 Q. Huang, Q. Niu, X.-F. Li, J. Liu, S.-N. Sun, L.-Z. Dong, S.-L. Li, Y.-P. Cai and Y.-Q. Lan, Demystifying the roles of single metal site and cluster in CO2 reduction via light and electric dual-responsive polyoxometalate-based metal-organic frameworks, *Sci. Adv.*, 2022, **8**, eadd5598.
42 D. A. Reddy, Y. Kim, M. Gopannagari, D. P. Kumar and T. K. Kim, Recent advances in metal–organic framework-based photocatalysts for hydrogen production, *Sustainable Energy Fuels*, 2021, **5**, 1597–1618.
43 M. Cheng, P. Yan, X. Zheng, B. Gao, X. Yan, G. Zhang, X. Cui and Q. Xu, Porphyrin-based Bi-MOFs with Enriched Surface Bi Active Sites for Boosting Photocatalytic CO2 Reduction, *Chem. – Eur. J.*, 2023, **29**, e202302395.
44 H.-Q. Xu, J. Hu, D. Wang, Z. Li, Q. Zhang, Y. Luo, S.-H. Yu and H.-L. Jiang, Visible-Light Photoreduction of CO2 in a Metal–Organic Framework: Boosting Electron–Hole Separation via Electron Trap States, *J. Am. Chem. Soc.*, 2015, **137**, 13440–13443.
45 S. Xie, C. Deng, Q. Huang, C. Zhang, C. Chen, J. Zhao and H. Sheng, Facilitated Photocatalytic CO2 Reduction in Aerobic Environment on a Copper-Porphyrin Metal–Organic Framework, *Angew. Chem., Int. Ed.*, 2023, **62**, e202216717.
46 K. Sun, Y. Qian and H.-L. Jiang, Metal-Organic Frameworks for Photocatalytic Water Splitting and CO2 Reduction, *Angew. Chem., Int. Ed.*, 2023, **62**, e202217565.
47 S. Shang, W. Xiong, C. Yang, B. Johannessen, R. Liu, H. Hsu, Q. Gu, M. Leung and J. Shang, Atomically Dispersed Iron Metal Site in a Porphyrin-Based Metal-Organic Framework for Photocatalytic Nitrogen Fixation, *ACS Nano*, 2021, **15**, 9670–9678.
48 J. Dong, D. Zhao, Y. Lu and W.-Y. Sun, Photoluminescent metal–organic frameworks and their application for sensing biomolecules, *J. Mater. Chem. A*, 2019, **7**, 22744–22767.
49 N. Kolobov, M. G. Goesten and J. Gascon, Metal–Organic Frameworks: Molecules or Semiconductors in

Photocatalysis?, *Angew. Chem., Int. Ed.*, 2021, **60**, 26038–26052.

50 Q. Wang and K. Domen, Particulate Photocatalysts for Light-Driven Water Splitting: Mechanisms, Challenges, and Design Strategies, *Chem. Rev.*, 2020, **120**, 919–985.

51 H. Nishiyama, T. Yamada, M. Nakabayashi, Y. Maehara, M. Yamaguchi, Y. Kuromiya, Y. Nagatsuma, H. Tokudome, S. Akiyama, T. Watanabe, R. Narushima, S. Okunaka, N. Shibata, T. Takata, T. Hisatomi and K. Domen, Photocatalytic solar hydrogen production from water on a 100-m2 scale, *Nature*, 2021, **598**, 304–307.

52 A. Fujishima and K. Honda, Electrochemical Photolysis of Water at a Semiconductor Electrode, *Nature*, 1972, **238**, 37–38.

53 H. Hu, Z. Wang, L. Cao, L. Zeng, C. Zhang, W. Lin and C. Wang, Metal–organic frameworks embedded in a liposome facilitate overall photocatalytic water splitting, *Nat. Chem.*, 2021, **13**, 358–366.

54 S. Dai, E Montero-Lanzuela, A. Tissot, H. G. Baldoví, H. García, S. Navalón and C. Serre, Room temperature design of Ce(IV)-MOFs: from photocatalytic HER and OER to overall water splitting under simulated sunlight irradiation, *Chem. Sci.*, 2023, **14**, 3451–3461.

55 C. Gomes Silva, I. Luz, F. X. Llabrés i Xamena, A. Corma and H. García, Water Stable Zr–Benzenedicarboxylate Metal–Organic Frameworks as Photocatalysts for Hydrogen Generation, *Chem. – Eur. J.*, 2010, **16**, 11133–11138.

56 A. A. Dhakshinamoorthy, A. M. Asiri and H. García, Metal-Organic Framework (MOF) Compounds: Photocatalysts for Redox Reactions and Solar Fuel Production, *Angew. Chem., Int. Ed.*, 2016, **55**, 5414–5445.

57 W. Wang, X. Xu, W. Zhou and Z. Shao, Recent Progress in Metal-Organic Frameworks for Applications in Electrocatalytic and Photocatalytic Water Splitting, *Adv. Sci.*, 2017, **4**, 1600371.

58 E. Hu, Y. Yao, Y. Cui and G. Qian, Strategies for the Enhanced Water Splitting Activity over Metal-Organic Frameworks-Based Electrocatalysts and Photocatalysts, *Mater. Today Nano*, 2021, **15**, 100124.

59 R. Jaryal, R. Kumar and S. Khullar, Mixed Metal-Metal Organic Frameworks (MM-MOFs) and Their Use as Efficient Photocatalystsfor Hydrogen Evolution from Water Splitting Reactions, *Coord. Chem. Rev.*, 2022, **464**, 214542.

60 K. Meyer, M. Ranocchiari and J. A. van Bokhoven, Metal Organic Frameworks for Photo-Catalytic Water Splitting, *Energy Environ. Sci.*, 2015, **8**, 1923–1937.

61 Y. Fang, Y. Ma, M. Zheng, P. Yang, A. M. Asiri and X. Wang, Metal-Organic Frameworks for Solar Energy Conversion by Photoredox Catalysis, *Coord. Chem. Rev.*, 2018, **373**, 83–115.

62 H. Luo, Z. Zeng, G. Zeng, C. Zhang, R. Xiao, D. Huang, C. Lai, M. Cheng, W. Wang, W. Xiong, Y. Yang, L. Qin, C. Zhou, H. Wang, Y. Zhou and S. Tian, Recent Progress on Metal-Organic Frameworks based- and Derived-Photocatalysts for Water Splitting, *Chem. Eng. J.*, 2020, **383**, 123196.

63 L. Lin, T. Hisatomi, S. Chen, T. Takata and K. Domen, Visible- Light-Driven Photocatalytic Water Splitting: Recent Progress and Challenges, *Trends Chem.*, 2020, **2**, 813–824.

64 P. Asselin and P. D. Harvey, Visible-Light-Driven Production of Solar Fuels Catalyzed by Nanosized Porphyrin-Based Metal–Organic Frameworks and Covalent–Organic Frameworks: A Review, *ACS Appl. Nano Mater.*, 2022, **5**, 6055–6082.

65 J.-D. Xiao and H.-L. Jiang, Metal–Organic Frameworks for Photocatalysis and Photothermal Catalysis, *Acc. Chem. Res.*, 2019, **52**, 356–366.

66 X. Fang, Q. Shang, Y. Wang, L. Jiao, T. Yao, Y. Li, Q. Zhang, Y. Luo and H. L. Jiang, Single Pt Atoms Confined into a Metal–Organic Framework for Efficient Photocatalysis, *Adv. Mater.*, 2018, **30**, 1705112.

67 F. Leng, H. Liu, M. Ding, Q.-P. Lin and H.-L. Jiang, Boosting Photocatalytic Hydrogen Production of Porphyrinic MOFs: The Metal Location in Metalloporphyrin Matters, *ACS Catal.*, 2018, **8**, 4583–4590.

68 Q. Zuo, T. Liu, C. Chen, Y. Ji, X. Gong, Y. Mai and Y. Zhou, Ultrathin Metal–Organic Framework Nanosheets with Ultrahigh Loading of Single Pt Atoms for Efficient Visible-Light-Driven Photocatalytic H2 Evolution, *Angew. Chem., Int. Ed.*, 2019, **58**, 10198–10203.

69 C. Lin, C. Han, H. Zhang, L. Gong, Y. Gao, H. Wang, Y. Bian, R. Li and J. Jiang, Porphyrin-Based Metal–Organic Frameworks for Efficient Photocatalytic H2 Production under Visible-Light Irradiation, *Inorg. Chem.*, 2021, **60**, 3988–3995.

70 H. Zhang, Q. Li, B. Li, B. Weng, Z. Tian, J. Yang, J. Hofkens, F. Lai and T. Liu, Atomically dispersed Pt sites on porous metal–organic frameworks to enable dual reaction mechanisms for enhanced photocatalytic hydrogen conversion, *J. Catal.*, 2022, **407**, 1–9.

71 G.-W. Guan, S.-T. Zheng, M. Xia, K.-X. Li, Y.-S. Ouyang, G. Yang and Q.-Y. Yang, Incorporating CdS and anchoring Pt single atoms into porphyrinic metal–organic frameworks for superior visible-light and sunlight-driven H2 evolution, *Chem. Eng. J.*, 2023, **464**, 142530.

72 S. Li, H.-M. Mei, S.-L. Yao, Z.-Y. Chen, Y.-L. Lu, L. Zhang and C.-Y. Su, Well-distributed Pt-nanoparticles within confined coordination interspaces of self-sensitized porphyrin metal–organic frameworks: synergistic effect boosting highly efficient photocatalytic hydrogen evolution reaction, *Chem. Sci.*, 2019, **10**, 10577–10585.

73 Z. Wu, L. Hou, W. Li, Q. Chen, C. Jin, Y. Chen, Q. Wei, H. Yang, Y. Jiang and D. Tang, Application of a novel biomimetic double-ligand zirconium-based metal organic framework in environmental restoration and energy conversion, *J. Colloid Interface Sci.*, 2022, **610**, 136–151.

74 K. Sasan, Q. Lin, C. Y. Mao and P. Feng, Incorporation of iron hydrogenase active sites into a highly stable metal–

organic framework for photocatalytic hydrogen generation, *Chem. Commun.*, 2014, **50**, 10390–10393.

75 X. Xu, Z. Zhang and X. Wang, Well-Defined Metal-Organic-Framework Hollow Nanostructures for Catalytic Reactions Involving Gases, *Adv. Mater.*, 2015, **27**, 5365–5371.

76 T. He, S. Chen, B. Ni, Y. Gong, Z. Wu, L. Song, L. Gu, W. Hu and X. Wang, Zirconium-Porphyrin-Based Metal-Organic Framework Hollow Nanotubes for Immobilization of Noble-Metal Single Atoms, *Angew. Chem., Int. Ed.*, 2018, **57**, 3493–3498.

77 L. Li, X. S. Wang, T. F. Liu and J. Ye, Titanium-Based MOF Materials: From Crystal Engineering to Photocatalysis, *Small Methods*, 2020, **4**, 2000486.

78 H. Feng, H. Li, X. Liu, Y. Huang, Q. Pan, R. Peng, R. Du, X. Zheng, Z. Yin, S. Li and Y. He, Porphyrin-based Ti-MOFs conferred with single-atom Pt for enhanced photocatalytic hydrogen evolution and NO removal, *Chem. Eng. J.*, 2022, **428**, 132045.

79 X. Wang, X. Zhang, W. Zhou, L. Liu, J. Ye and D. Wang, An ultrathin porphyrin-based metal-organic framework for efficient photocatalytic hydrogen evolution under visible light, *Nano Energy*, 2019, **62**, 250–258.

80 G. Lan, Y. Y. Zhu, S. S. Veroneau, Z. Xu, D. Micheroni and W. Lin, Electron Injection from Photoexcited Metal–Organic Framework Ligands to Ru2 Secondary Building Units for Visible-Light-Driven Hydrogen Evolution, *J. Am. Chem. Soc.*, 2018, **140**, 5326–5329.

81 J. S. Jang, H. G. Kim and J. S. Lee, Heterojunction Semiconductorbes: A Strategy to Develop Efficient Photocatalytic Materials for Visible Light Water Splitting, *Catal. Today*, 2012, **185**, 270–277.

82 J. Low, J. Yu, M. Jaroniec, S. Wageh and A. A. Al-Ghamdi, Heterojunction Photocatalysts, *Adv. Mater.*, 2017, **29**, 1601694.

83 S. J. A. Moniz, S. A. Shevlin, D. J. Martin, Z. X. Guo and J. Tang, Visible-Light Driven Heterojunction Photocatalysts for Water Splitting - A Critical Review, *Energy Environ. Sci.*, 2015, **8**, 731–759.

84 D. Ma, J. W. Shi, Z. Pu, S. Mao, X. Xu, D. He, R. Guo and F. Chen, Decorating Phosphorus-Doped g-C3N4 with Zinc Porphyrin Metal–Organic Framework via an Electrostatic Self-Assembly Process: An Efficient Strategy to Boost Photocatalytic Hydrogen Evolution Performance, *Sol. RRL*, 2022, **6**, 2200714.

85 Z. Pu, B. Xiao, S. Mao, Y. Sun, D. Ma, H. Wang, J. Zhou, Y. Cheng and J. W. Shi, An electron-hole separation mechanism caused by the pseudo-gap formed at the interfacial Co-N bond between cobalt porphyrin metal organic framework and boron-doped g-C3N4 for boosting photocatalytic H2 production, *J. Colloid Interface Sci.*, 2022, **628**, 477–487.

86 Y. Chen, W. Zhang, T. Zhang, W. Zhang, L. Qin, S. Z. Kang and X. Li, A special nano-micro hybrid anchored porphyrin metal-organic framework for enhanced photocatalytic hydrogen generation, *J. Alloys Compd.*, 2022, **926**, 166980.

87 H. Zhu, L. Qin, Z. Wei, T. Zhang, S.-Z. Kang and X. Li, An in-situ assembled titanate nanotube-based dimensionality-hybrid for enhanced photocatalytic hydrogen generation, *Appl. Surf. Sci.*, 2023, **619**, 156795.

88 P. Jin, L. Wang, X. Ma, R. Lian, J. Huang, H. She, M. Zhang and Q. Wang, Construction of hierarchical ZnIn2S4@PCN-224 heterojunction for boosting photocatalytic performance in hydrogen production and degradation of tetracycline hydrochloride, *Appl. Catal., B*, 2021, **284**, 119762.

89 W. Zhang, Y. Chen, Y. Deng, T. Zhang, L. Qin, S. Z. Kang and X. Li, Two dimensional porphyrin-based metal–organic framework constructed on K4Nb6O17 microflowers for highly efficient charge transfer and photocatalytic hydrogen generation, *Appl. Surf. Sci.*, 2022, **599**, 153922.

90 Z. Xia, R. Yu, H. Yang, B. Luo, Y. Huang, D. Li, J. Shi and D. Xu, Novel 2D Zn-porphyrin metal organic frameworks revived CdS for photocatalysis of hydrogen production, *Int. J. Hydrogen Energy*, 2022, **47**, 13340–13350.

91 Y.-N. Gong, X. Guan and H.-L. Jiang, Covalent organic frameworks for photocatalysis: Synthesis, structural features, fundamentals and performance, *Coord. Chem. Rev.*, 2023, **475**, 214889.

92 J. Ding, X. Guan, J. Lv, X. Chen, Y. Zhang, H. Li, D. Zhang, S. Qiu, H.-L. Jiang and Q. Fang, Three-Dimensional Covalent Organic Frameworks with Ultra-Large Pores for Highly Efficient Photocatalysis, *J. Am. Chem. Soc.*, 2023, **145**, 3248–3254.

93 X. Li, Q. Dong, Q. Tian, A. Sial, H. Wang, H. Wen, B. Pan, K. Zhang, J. Qin and C. Wang, Recent advance in metal- and covalent-organic framework-based photocatalysis for hydrogen evolution, *Mater. Today Chem.*, 2022, **26**, 101037.

94 Y. Wang, X. Wang and M. Antonietti, Polymeric graphitic carbon nitride as a heterogeneous organocatalyst: From photochemistry to multipurpose catalysis to sustainable chemistry, *Angew. Chem., Int. Ed.*, 2012, 68–89.

95 J. Fu, J. Fu, C. Jiang and B. Cheng, g-C3N4-Based Heterostructured Photocatalysts, *Adv. Energy Mater.*, 2018, **8**, 1701503.

96 H. Feng, H. Li, X. Liu, Y. Huang, Q. Pan, R. Peng, R. Du, X. Zheng, Z. Yin, S. Li and Y. He, Porphyrin-based Ti-MOFs conferred with single-atom Pt for enhanced photocatalytic hydrogen evolution and NO removal, *Chem. Eng. J.*, 2022, **428**, 13205.

97 C. M. Rueda-Navarro, B. Ferrer, H. G. Baldoví and S. Navalón, Photocatalytic Hydrogen Production from Glycerol Aqueous Solutions as Sustainable Feedstocks Using Zr-Based UiO-66 Materials under Simulated Sunlight Irradiation, *Nanomaterials*, 2022, **12**, 3808.

98 Y. An, Y. Liu, P. An, J. Dong, B. Xu, Y. Dai, X. Qin, X. Zhang, M. H. Whangbo and B. Huang, NiII Coordination to Al-Based Metal- Organic Framework

Made from 2-Aminoterephthalate for Photocatalytic Overall Water Splitting, *Angew. Chem., Int. Ed.*, 2017, **56**, 3036–3040.

99 S. Remiro-Buenamañana, M. Cabrero-Antonino, M. Martínez-Guanter, M. Álvaro, S. Navalón and H. García, Influence of co-catalysts on the photocatalytic activity of MIL-125(Ti)-NH2 in the overall water splitting, *Appl. Catal., B*, 2019, **254**, 677–684.

100 Y. An, B. Xu, Y. Liu, Z. Wang, P. Wang, Y. Dai, X. Qin, X. Zhang and B. Huang, Photocatalytic Overall Water Splitting over MIL-125(Ti) upon CoPi and Pt Co-catalyst Deposition, *ChemistryOpen*, 2017, **6**, 701–705.

101 A. Melillo, M. Cabrero-Antonino, S. Navalón, M. Álvaro, B. Ferrer and H. García, Enhancing visible-light photocatalytic activity for overall water splitting in UiO-66 by controlling metal node composition, *Appl. Catal., B*, 2020, **278**, 119345.

102 J. Zhang, T. Bai, H. Huang, M. H. Yu, X. Fan, Z. Chang and X. H. Bu, Metal-Organic-Framework-Based Photocatalysts Optimized by Spatially Separated Cocatalysts for Overall Water Splitting, *Adv. Mater.*, 2020, **32**, 2004747.

103 P. Salcedo-Abraira, A. A. Babaryk, E. Montero-Lanzuela, O. R. Contreras-Almengor, M. Cabrero-Antonino, E. S. Svensson Grape, T. Willhammar, S. Navalón, E. Elkäim, H. García and P. Horcajada, A novel porous Ti-Squarate as Efficient Photocatalyst in the Overall Water Splitting Reaction under Simulated Sunlight Irradiation, *Adv. Mater.*, 2021, **33**, 2106627.

104 P. Salcedo-Abraira, S. M. F. Vilela, A. A. Babaryk, M. Cabrero-Antonino, P. Gregorio, F. Salles, S. Navalon, H. Garcia and P. Horcajada, Nickel phosphonate MOF as efficient water splitting photocatalyst, *Nano Res.*, 2021, **14**, 450–457.

105 X.-P. Wu, L. Gagliardi and D. G. Truhlar, Cerium Metal-Organic Framework for Photocatalysis, *J. Am. Chem. Soc.*, 2018, **140**, 7904–7912.

106 X.-P. Wu, L. Gagliardi and D. G. Truhlar, Metal Doping in Cerium Metal-Organic Frameworks for Visible-Response Water Splitting Photocatalysts, *J. Chem. Phys.*, 2019, **150**, 041701.

107 A. Melillo, M. Cabrero-Antonino, B. Ferrer, A. Dhakshinamoorthy, H. G. Baldoví and S. Navalón, MOF-on-MOF Composites with UiO-66-Based Materials as Photocatalysts for the Overall Water Splitting under Sunlight Irradiation, *Energy Fuels*, 2023, **37**, 5457–5468.

108 T. G. Semerci, A. Melillo, Y. Ç. Mutlu and H. Garcia, Band alignment of PCN-222 via selection of the metal porphyrin linker for sunlight driven photocatalytic overall water splitting, *Catal. Today*, 2023, **423**, 113931.

109 B. Gikonyo, E. Montero-Lanzuela, H. Baldovi, S. De, C. Journet, T. Devic, N. Guillou, D. Tiana, S. Navalon and A. Fateeva, Mixed-metal Zr/Ti MIL-173 porphyrinic metal-organic frameworks as efficient photocatalysts towards solar-driven overall water splitting, *J. Mater. Chem. A*, 2022, **10**, 24938–24950.

110 T. G. Semerci, A. Melillo, Y.Ç Mutlu and H. Garcia, Band alignment of PCN-222 via selection of the metal porphyrin linker for sunlight driven photocatalytic overall water splitting, *Catal. Today*, 2022, 113931.

111 A. Mukhopadhyay, S. Duttagupta and A. Mukherjee, Emerging organic contaminants in global community drinking water sources and supply: A review of occurrence, processes and remediation, *J. Environ. Chem. Eng.*, 2022, **10**, 107560.

112 Directive, Directive (EU) 2020/2184 of the European Parliament and of the Council of 16 December 2020 on the quality of water intended for human consumption, *Off. J. Eur. Union*, 2020, **2019**, 1–62.

113 L. Comoretto and S. Chiron, Comparing pharmaceutical and pesticide loads into a small Mediterranean river, *Sci. Total Environ.*, 2005, **349**, 201–210.

114 J. L. Acero, F. J. Benitez, F. J. Real, G. Roldan and E. Rodriguez, Chlorination and bromination kinetics of emerging contaminants in aqueous systems, *Chem. Eng. J.*, 2013, **219**, 43–50.

115 E. A. Serna-Galvis, J. Porras and R. A. Torres-Palma, A critical review on the sonochemical degradation of organic pollutants in urine, seawater, and mineral water, *Ultrason. Sonochem.*, 2022, **82**, 105861.

116 L. A. Galeano, M.Á Vicente and A. Gil, Catalytic degradation of organic pollutants in aqueous streams by mixed Al/M-pillared clays (M = Fe, Cu, Mn), *Catal. Rev. - Sci. Eng.*, 2014, **56**, 239–287.

117 E. Haque, J. E. Lee, I. T. Jang, Y. K. Hwang, J. S. Chang, J. Jegal and S. H. Jhung, Adsorptive removal of methyl orange from aqueous solution with metal-organic frameworks, porous chromium-benzenedicarboxylates, *J. Hazard. Mater.*, 2010, **181**, 535–542.

118 M. Alvaro, E. Carbonell, B. Ferrer, F. X. Llabrés i Xamena and H. Garcia, Semiconductor behavior of a metal-organic framework (MOF), *Chem. – Eur. J.*, 2007, **13**, 5106–5112.

119 H. L. B. Boström, S. Emmerling, F. Heck, C. Koschnick, A. J. Jones, M. J. Cliffe, R. Al Natour, M. Bonneau, V. Guillerm, O. Shekhah, M. Eddaoudi, J. Lopez-Cabrelles, S. Furukawa, M. Romero-Angel, C. Martí-Gastaldo, M. Yan, A. J. Morris, I. Romero-Muñiz, Y. Xiong, A. E. Platero-Prats, J. Roth, W. L. Queen, K. S. Mertin, D. E. Schier, N. R. Champness, H. H.-M. Yeung and B. V. Lotsch, How reproducible is the synthesis of Zr–porphyrin metal–organic frameworks? An interlaboratory study, *Adv. Mater.*, 2023, 2304832.

120 Society, The impact of textile production and waste on the environment (infographics), *Eur. Parliam.*, 2020, pp. 1–7.

121 Y. Zhao, Y. Dong, F. Lu, C. Ju, L. Liu, J. Zhang, B. Zhang and Y. Feng, Coordinative integration of a metal-porphyrinic framework and TiO2 nanoparticles for the formation of composite photocatalysts with enhanced visible-light-driven photocatalytic activities, *J. Mater. Chem. A*, 2017, **5**, 15380–15389.

122 Z. H. Zhu, Y. Liu, C. Song, Y. Hu, G. Feng and B. Z. Tang, Porphyrin-Based Two-Dimensional Layered Metal-Organic

Framework with Sono-/Photocatalytic Activity for Water Decontamination, *ACS Nano*, 2022, **16**, 1346–1357.

123 S. Zhao, S. Li, Z. Zhao, Y. Su, Y. Long, Z. Zheng, D. Cui, Y. Liu, C. Wang, X. Zhang and Z. Zhang, Microwave-assisted hydrothermal assembly of 2D copper-porphyrin metal-organic frameworks for the removal of dyes and antibiotics from water, *Environ. Sci. Pollut. Res.*, 2020, **27**, 39186–39197.

124 C. N. C. Hitam and A. A. Jalil, A review on exploration of Fe2O3 photocatalyst towards degradation of dyes and organic contaminants, *J. Environ. Manage.*, 2020, **258**, 110050.

125 J. Rodrigues, T. Hatami, J. M. Rosa, E. B. Tambourgi and L. H. I. Mei, Photocatalytic degradation using ZnO for the treatment of RB 19 and RB 21 dyes in industrial effluents and mathematical modeling of the process, *Chem. Eng. Res. Des.*, 2020, **153**, 294–305.

126 V. Shanmuganathan, J. Santhosh Kumar, R. Pachaiappan and P. Thangadurai, Transition metal ion-doped In2O3nanocubes: investigation of their photocatalytic degradation activity under sunlight, *Nanoscale Adv.*, 2021, **3**, 471–485.

127 S. Abdpour, E. Kowsari, M. R. Alavi Moghaddam, L. Schmolke and C. Janiak, Mil-100(Fe) nanoparticles supported on urchin like Bi2S3 structure for improving photocatalytic degradation of rhodamine-B dye under visible light irradiation, *J. Solid State Chem.*, 2018, **266**, 54–62.

128 Y. Xia, S. Shang, X. Zeng, J. Zhou and Y. Li, A Novel Bi2MoO6/ZIF-8 Composite for Enhanced Visible Light Photocatalytic Activity, *Nanomaterials*, 2019, **9**, 545.

129 R. Hariri and S. Dehghanpour, Adsorptive removal and visible-light photocatalytic degradation of large cationic and anionic dyes induced by air-bubbles in the presence of a magnetic porphyrinic metal-organic framework (Fe3O4@SiO_2@PCN-222(Fe)), *J. Phys. Chem. Solids*, 2021, **155**, 110126.

130 Z. Xia, B. Shi, W. Zhu and C. Lü, Temperature-responsive polymer-tethered Zr-porphyrin MOFs encapsulated carbon dot nanohybrids with boosted visible-light photodegradation for organic contaminants in water, *Chem. Eng. J.*, 2021, **426**, 131794.

131 N. Wang, S. Liu, Z. Sun, Y. Han, J. Xu, Y. Xu, J. Wu, H. Meng, B. Zhang and X. Zhang, Synergistic adsorption and photocatalytic degradation of persist synthetic dyes by capsule-like porphyrin-based MOFs, *Nanotechnology*, 2021, **32**, 465705.

132 J. Xue, M. Xu, J. Gao, Y. Zong, M. Wang and S. Ma, Multifunctional porphyrinic Zr-MOF composite membrane for high-performance oil-in-water separation and organic dye adsorption/photocatalysis, *Colloids Surf., A*, 2021, **628**, 127288.

133 M. Kim, J. S. Oh, B. H. Kim, A. Y. Kim, K. C. Park, J. Mun, G. Gupta and C. Y. Lee, Enhanced Photocatalytic Performance of Nanosized Mixed-Ligand Metal-Organic Frameworks through Sequential Energy and Electron Transfer Process, *Inorg. Chem.*, 2020, **59**, 12947–12953.

134 A. Guo, X. Wang, H. Liu, X. Li, L. Yang and W. Yang, Efficient photocatalytic degradation of water contaminants via Ag decorated porphyrin-based organic framework materials, *Surf. Interfaces*, 2023, **38**, 102843.

135 J. Mu, S. Li, J. Wang, X. Li, W. Chen, X. Tong, Y. Tang and L. Li, Efficient catalytic ozonation of bisphenol A by three-dimensional mesoporous CeOx-loaded SBA-16, *Chemosphere*, 2021, **278**, 130412.

136 T. Huang, L. A. Danaher, B. J. Brüschweiler, G. E. N. Kass and C. Merten, Naturally occurring bisphenol F in plants used in traditional medicine, *Arch. Toxicol.*, 2019, **93**, 1485–1490.

137 G. M. Klečka, C. A. Staples, K. E. Clark, N. Van Der Hoeven, D. E. Thomas and S. G. Hentges, Exposure analysis of bisphenol A in surface water systems in North America and Europe, *Environ. Sci. Technol.*, 2009, **43**, 6145–6150.

138 C. Zhang, W. Fei, H. Wang, N. Li, D. Chen, Q. Xu, H. Li, J. He and J. Lu, p-n Heterojunction of BiOI/ZnO nanorod arrays for piezo-photocatalytic degradation of bisphenol A in water, *J. Hazard. Mater.*, 2020, **399**, 123109.

139 Z. Wang, Z. Liu, J. Huang, Y. Chen, R. Su, J. He, G. Lv, B. Gao, W. Zhou, Y. Wang, Z. Wang and Q. Li, Zr6O8-porphyrinic MOFs as promising catalysts for the boosting photocatalytic degradation of contaminants in high salinity wastewater, *Chem. Eng. J.*, 2022, **440**, 135883.

140 Y. Xiang, X. Wang, X. Zhang, H. Hou, K. Dai, Q. Huang and H. Chen, Enhanced visible light photocatalytic activity of TiO2 assisted by organic semiconductors: A structure optimization strategy of conjugated polymers, *J. Mater. Chem. A*, 2017, **6**, 153–159.

141 J. Li, X. Li, G. Wu, J. Guo, X. Yin and M. Mu, Construction of 2D Co-TCPP MOF decorated on B-TiO2−X nanosheets: Oxygen vacancy and 2D–2D heterojunctions for enhancing visible light-driven photocatalytic degradation of bisphenol A, *J. Environ. Chem. Eng.*, 2021, **9**, 106723.

142 Z. Wang, Q. Li, R. Su, G. Lv, Z. Wang, B. Gao and W. Zhou, Enhanced degradation of bisphenol F in a porphyrin-MOF based visible-light system under high salinity conditions, *Chem. Eng. J.*, 2022, **428**, 132106.

143 P. Chaturvedi, P. Shukla, B. S. Giri, P. Chowdhary, R. Chandra, P. Gupta and A. Pandey, Prevalence and hazardous impact of pharmaceutical and personal care products and antibiotics in environment: A review on emerging contaminants, *Environ. Res.*, 2021, **194**, 110664.

144 I. C. Vasilachi, D. M. Asiminicesei, D. I. Fertu and M. Gavrilescu, Occurrence and fate of emerging pollutants in water environment and options for their removal, *Water*, 2021, **13**, 1–34.

145 A. J. Ebele, M. A.-E. Abdallah and S. Harrad, Pharmaceuticals and personal care products (PPCPs) in the freshwater aquatic environment, *Emerging Contam.*, 2017, **3**, 1–16.

146 T. Backhaus, Commentary on the EU Commission's proposal for amending the Water Framework Directive, the Groundwater Directive, and the Directive on

Environmental Quality Standards, *Environ. Sci. Eur.*, 2023, **35**, 22.

147 W.-Q. Li, Y.-X. Wang, J.-Q. Chen, N.-N. Hou, Y.-M. Li, X.-C. Liu, R.-R. Ding, G.-N. Zhou, Q. Li, X.-G. Zhou and Y. Mu, Boosting photo-Fenton process enabled by ligand-to-cluster charge transfer excitations in iron-based metal organic framework, *Appl. Catal., B*, 2022, **302**, 120882.

148 J. Hu, S. Wang, J. Yu, W. Nie, J. Sun and S. Wang, Duet Fe3C and FeNxSites for H_2O_2Generation and Activation toward Enhanced Electro-Fenton Performance in Wastewater Treatment, *Environ. Sci. Technol.*, 2021, **55**, 1260–1269.

149 United States Enviornmental Protection Agency, Secondary Drinking Water Standards: Guidance for Nuisance Chemicals, **https://www.epa.gov/sdwa/secondary-drinking-water-standards-guidance-nuisance-chemicals**, (accessed 24 July 2023).

150 Y. Zong, S. Ma, J. Gao, M. Xu, J. Xue and M. Wang, Synthesis of Porphyrin Zr-MOFs for the Adsorption and Photodegradation of Antibiotics under Visible Light, *ACS Omega*, 2021, **6**, 17228–17238.

151 X. Zhang, Z. Liu, B. Shao, T. Wu, Y. Pan, S. Luo, M. He, L. Ge, J. Sun, C. Cheng and J. Huang, Construction of ZnIn2S4/MOF-525 heterojunction system to enhance photocatalytic degradation of tetracycline, *Environ. Sci. Pollut. Res.*, 2023, 67647–67661.

152 S. Yuan, J.-S. Qin, L. Zou, Y.-P. Chen, X. Wang, Q. Zhang and H.-C. Zhou, Thermodynamically Guided Synthesis of Mixed-Linker Zr-MOFs with Enhanced Tunability, *J. Am. Chem. Soc.*, 2016, **138**, 6636–6642.

153 Y. Gao, J. Xia, D. Liu, R. Kang, G. Yu and S. Deng, Synthesis of mixed-linker Zr-MOFs for emerging contaminant adsorption and photodegradation under visible light, *Chem. Eng. J.*, 2019, **378**, 122118–122118.

154 X. Gan, X. Li and B. Wang, Adsorption and degradation of multiple micropollutants with trace concentrations by porous Zr-porphyrin metal-organic frameworks with missing linker defects in water, *Microporous Mesoporous Mater.*, 2023, **349**, 112444.

155 Z. Wang, J. Huang, W. Wang, X. Wang, Y. Wang, B. Gao and Q. Li, Removal of norfloxacin from high salinity wastewater by Hf-porphyrin MOF with missing linker defects: Insights into anion trapping and photoinduced charge transfer effects, *Chem. Eng. J.*, 2023, **466**, 143194–143194.

156 Y. Gao, M. J. Suh, J. H. Kim and G. Yu, Imparting Multifunctionality in Zr-MOFs Using the One-Pot Mixed-Linker Strategy: The Effect of Linker Environment and Enhanced Pollutant Removal, *ACS Appl. Mater. Interfaces*, 2022, **14**, 24351–24362.

157 S. Rengaraj, S. Venkataraj, J. W. Yeon, Y. Kim, X. Z. Li and G. K. H. Pang, Preparation, characterization and application of Nd-TiO2 photocatalyst for the reduction of Cr(VI) under UV light illumination, *Appl. Catal., B*, 2007, **77**, 157–165.

158 Y. Ku and I. L. Jung, Photocatalytic reduction of Cr(VI) in aqueous solutions by UV irradiation with the presence of titanium dioxide, *Water Res.*, 2001, **35**, 135–142.

159 H. Hossini, B. Shafie, A. D. Niri, M. Nazari, A. J. Esfahlan, M. Ahmadpour, Z. Nazmara, M. Ahmadimanesh, P. Makhdoumi, N. Mirzaei and E. Hoseinzadeh, A comprehensive review on human health effects of chromium: insights on induced toxicity, *Environ. Sci. Pollut. Res.*, 2022, **29**, 70686–70705.

160 N. Sharma, A. K. Dey, R. Y. Sathe, A. Kumar, V. Krishnan, T. J. D. Kumar and C. M. Nagaraja, Highly efficient visible-light-driven reduction of Cr(vi) from water by porphyrin-based metal-organic frameworks: Effect of band gap engineering on the photocatalytic activity, *Catal. Sci. Technol.*, 2020, **10**, 7724–7733.

161 D. Chen, W. Liu, Z. Guo, Z. Jin, B. Li and H. Xing, Visible-Light-Driven Sonophotocatalysis for the Rapid Reduction of Aqueous Cr(VI) Based on Zirconium-Porphyrin Metal-Organic Frameworks with csq Topology, *Inorg. Chem.*, 2021, **60**, 18133–18140.

162 P. K. Pandey, P. H. Kass, M. L. Soupir, S. Biswas and V. P. Singh, Contamination of water resources by pathogenic bacteria, *AMB Express*, 2014, **4**, 51.

163 G. Zhang, W. Li, S. Chen, W. Zhou and J. Chen, Problems of conventional disinfection and new sterilization methods for antibiotic resistance control, *Chemosphere*, 2020, **254**, 126831.

164 R. Gupta and J. Modak, Bacterial Lysis via Photocatalysis - A Critical Mechanistic Review, *ChemCatChem*, 2020, **12**, 2148–2170.

165 Z. Liang, H. Wang, K. Zhang, G. Ma, L. Zhu, L. Zhou and B. Yan, Oxygen-defective MnO_2/ZIF-8 nanorods with enhanced antibacterial activity under solar light, *Chem. Eng. J.*, 2022, **428**, 131349.

166 S. Aftab, T. Shabir, A. Shah, J. Nisar, I. Shah, H. Muhammad and N. Shah, Highly Efficient Visible Light Active Doped ZnO Photocatalysts for the Treatment of Wastewater Contaminated with Dyes and Pathogens of Emerging Concern, *Nanomaterials*, 2022, **12**, 486.

167 Y.-L. Li, J.-F. Ai, Z.-C. Chen, H.-L. Wang, Z.-H. Zhu, F.-P. Liang and H.-H. Zou, Multiple Strategies Enhance the ROS of Metal–Organic Frameworks for Energy-Efficient Photocatalytic Water Purification and Sterilization, *ACS Mater. Lett.*, 2023, **5**, 1317–1331.

168 Y. Luo, X. Liu, L. Tan, Z. Li, K. W. K. Yeung, Y. Zheng, Z. Cui, Y. Liang, S. Zhu, C. Li, X. Wang and S. Wu, Enhanced photocatalytic and photothermal properties of ecofriendly metal-organic framework heterojunction for rapid sterilization, *Chem. Eng. J.*, 2021, **405**, 126730.

169 L. Chen, D. Li, Y. Wang and C. Duan, Highly efficient solar steam generation of supported metal–organic framework membranes by a photoinduced electron transfer process, *Nanoscale*, 2019, **11**, 11121–11127.

170 L. I. U. Qiang and G. U. O. CanCheng, Theoretical studies and industrial applications of oxidative activation of inert

C-H bond by metalloporphyrin-based biomimetic catalysis, *Sci. China: Chem.*, 2012, **55**, 2036–2053.

171 J. Turconi, F. Griolet, R. Guevel, G. Oddon, R. Villa, A. Geatti, M. Hvala, K. Rossen, R. Göller and A. Burgard, Semisynthetic Artemisinin, the Chemical Path to Industrial Production, *Org. Process Res. Dev.*, 2014, **18**, 417–422.

172 N.-C. Chiu, M. T. Nord, L. Tang, L. S. Lancaster, J. S. Hirschi, S. K. Wolff, E. M. Hutchinson, K. A. Goulas, W. F. Stickle, T. J. Zuehlsdorff, C. Fang and K. C. Stylianou, Designing Dual-Functional Metal–Organic Frameworks for Photocatalysis, *Chem. Mater.*, 2022, **34**, 8798–8807.